AIAA/AAS Astrodynamics Specialist Conference
13 - 16 August 2012, Minneapolis, Minnesota

AIAA 2012-4745

Long-term Dynamics of HAMR Objects in HEO

Aaron Rosengren,* Daniel Scheeres†
University of Colorado at Boulder, Boulder, CO 80309

The dynamics of high area-to-mass ratio (HAMR) objects in high-Earth orbit have been explored in recent years, finding that extreme variations occur in eccentricity and inclination due to the combined effects of solar radiation pressure, higher harmonics of the Earth gravity field, and lunisolar perturbations. A sound understanding of their nature, orbital evolution, and possible origin is critical for space situational awareness. We explore a new averaged model for the orbital evolution of HAMR objects, explicitly given in terms of the eccentricity and angular momentum vectors. This new formulation accounts for all relevant perturbations and provides predictions of the long-term orbital evolution of HAMR objects that compare well with non-averaged numerical integrations over many decades. In this paper we present the force models for each perturbation, their fundamental predictions, and make comparisons with explicit long-term numerical integrations of HAMR objects in GEO space. We find that many of the extreme dynamical behaviors reported for these objects are attributable to the complex coupling between SRP, J2 and lunisolar perturbations. The dynamical configuration of the Earth-Moon-Sun system, and in particular the regression of the lunar node in the ecliptic plane, was found to have a significant resonant effect on the long-term dynamics of HAMR debris orbits.

I. Introduction

THE motion of high area-to-mass ratio (HAMR) objects in high-Earth orbits (HEO) has been studied extensively since the discovery of this debris population in near GEO orbits by Schildknecht and colleagues (ca. 2004). Anselmo and Pardini have made several numerical investigations of this problem, mapping out the dynamics of these objects over long timespans with all relevant perturbations included. Their most recent work[1] presents a detailed analysis concerning the long-term evolution of HAMR debris in HEO subject to solar radiation pressure (SRP), geopotential harmonics up to degree and order eight, and third-body gravitational interactions induced by the Sun and the Moon. Valk *et al.*[24] study this problem using techniques from classical perturbation analysis, and are able to analytically approximate the solutions to the SRP averaged equations and then successfully include terms due to the Earth oblateness (J_2), and potentially to include other perturbations.

In the framework of orbit propagation, the evolution of space debris objects, taking into account both short-period and long-period terms, requires numerical integration of the precise set of differential equations, and the investigation of a broad range of possible parameter values. However, such computations become very costly when continuously applied over a period of several decades, as is necessary in the case of HAMR debris. It therefore seems reasonable to investigate the equations that govern the long-term behavior of orbits; such equations can be derived by the method of averaging. The method of averaging, developed by Krylov and Bogoliubov[9] in the analysis of nonlinear oscillations, and generalized by Bogoliubov and Mitropolsky,[2] was first applied to problems in celestial mechanics and satellite theory in the early 1960s.[11,13,23] The averaged equations of motion capture the secular evolution of the system and can be numerically integrated, with significantly reduced computational requirements, or in some cases, solved in closed form (cf.,[15,18,19]). The advantage of this approach is that it is possible to easily capture the qualitative effect of

*Graduate Research Associate, H. Joseph Smead Fellow, Department of Aerospace Engineering Sciences, 429 UCB, Boulder, CO, 80309, Student Member AIAA
†A. Richard Seebass Endowed Chair Professor, Department of Aerospace Engineering Sciences, 429 UCB, Boulder, CO, 80309, Associate Fellow AIAA

perturbations over long timespans, and it reveals the essential dependence of the evolution on the system parameters in a more satisfactory way than does a numerical solution of the non-averaged equations.

The Draper Semi-analytical Satellite Theory (DSST) orbit propagator, developed by Cefola *et al.*, replaces the conventional equations of motion with two formulas: equations of motion for the mean equinoctial elements, and expressions for the short-periodic motion in the equinoctial elements.[3,14] Very complete force models have been developed for the averaged equations and for the short-periodic motion.[4,7] Liou and Weaver used PROP3D, a fast orbit propagator based on the averaging principle that was developed for NASA's debris evolutionary models, to investigate the HAMR debris problem.[12] PROP3D, while not as complete as DSST, accounts for the perturbations from Earth gravity due to the J_2, J_3, and J_4 zonal harmonics, low-order lunisolar gravitational perturbations, and SRP with Earth's shadow effects. Through comparisons with a high-fidelity orbit integrator, they showed that HAMR objects in GEO are dominated by major perturbations, not those of higher order. Chao (2006) performed long-term studies of the orbital evolution of GEO objects with high area-to-mass ratios, through analytically averaged equations.[5] Chao investigated the secular effects of SRP on the eccentricity and argument of perigee by averaging over the period of the HAMR object about the Earth. The long-term motion of the orbit inclination and longitude of the ascending node were studied though doubly-averaged equations for the lunisolar attraction, ignoring higher-order terms in eccentricity, and singly-averaged equations for the SRP perturbation.

In previous papers, we explored a new averaged model for the evolution of HAMR debris orbits at high altitudes (such as GEO), explicitly given in terms of the eccentricity and angular momentum vectors.[18,19,21] The qualitative behavior underlined by our combined theory of SRP and J_2 is in good agreement with the numerical integrations of earlier researchers.[1,5,12,24] The SRP-only theory is sufficient to capture the sub-yearly oscillations in the inclination evolution that ride on top of the longer-term drift, and the shift in the long-term oscillation periods with changing area-to-mass. Incorporating J_2 into our SRP-only theory has, as a consequence, a reduction in both the amplitudes and periods of the long-term secular drift in inclination. The high-fidelity propagations predict that the long-term inclination and eccentricity variations have a varying maximum amplitude.[1] We attribute these non-periodic variations largely to the effects of third-body perturbations, which is the topic specifically addressed here.

This paper aims to provide a general and qualitative understanding of the orbital motion of HAMR objects released in high-Earth orbits subject to the averaged effects of solar radiation pressure, Earth oblateness, and lunisolar gravitational attraction. We derive singly- and doubly-averaged expressions for third-body perturbations, which are valid for all eccentricity and all inclination, and incorporate them into our previous theory. In this formulation, we adopt a more general perspective that is independent of any particular system of reference by adhering to vector and dyadic notation. The major contribution of this work is in the analytical representation of the averaged equations in terms of the Gauss equations. This paper is organized into the following discussions. We first present the environment and force models for each perturbation, and discuss any underlying assumptions and approximations. We then formulate the Gauss perturbation equations in alternate osculating orbital elements, and fully derive the averaged equations of motion. Following this we demonstrate the validity of the averaged equations by comparing numerical integrations of them to integrations of the exact Newtonian equations. The extent to which the qualitative properties of the orbit persist with increasing area-to-mass is investigated. We show how the geometry of the Earth-Moon-Sun system, and in particular the lunar nodal regression, causes a resonance effect with a particular class of HAMR objects leading to complex evolutionary behavior. Finally, we discuss our future research directions, which includes using our new averaged model to make predictions of the global spatiotemporal distribution of the HAMR debris population.

II. Environment and Force Models

A. The Earth-Moon-Sun System

Any account of the motions in the Earth-Moon-Sun systems has to start with a description of the dynamical configuration of this three-body problem. Perozzi et al. (1991),[16] using eclipse records, the JPL ephemeris, and results from numerical integration of the three-body problem, showed that the mean geometry of the Earth-Moon-Sun system repeats itself closely after a period of time equal in length to the classical eclipse prediction cycle known as the Saros. Saros means repetition, and indicates a period of 223 synodic months (6585.3213 days, or 18 years 10/11 days, dependent on the number of leap-years within the cycle), after which the Sun has returned to the same place it occupied with respect to the nodes of the Moon's orbit when the cycle began. While the motion of the Earth around the Sun can, over timespans of interest, be considered Keplerian, the Moon is subject to consistent solar perturbations resulting in periodic and secular variations of its orbital elements. The node of the Moon's orbital plane regresses in the ecliptic plane with a sidereal period of 6798.3 days (about 18.61 years); the node moving westward on the ecliptic at a rate of roughly 1° in 18.9 days. Thus, the Saros is shorter, by about 213 days, than the sidereal period of nodal regression.

The intrinsic complexity of lunar motion must be taken into account for long-term studies of HAMR objects.

To describe the motion of the Earth about the Sun, we define a heliocentric orbit frame, $(\hat{\boldsymbol{E}}_e, \hat{\boldsymbol{E}}_{e_\perp}, \hat{\boldsymbol{H}}_e)$, in which $\hat{\boldsymbol{E}}_e$ is the unit vector pointing to the orbit perihelion, $\hat{\boldsymbol{E}}_{e_\perp}$ is the unit vector in the heliocentric plane of motion and normal to $\hat{\boldsymbol{E}}_e$, and the cross product of these two vectors defines the orbit normal, specified as $\hat{\boldsymbol{H}}_e$, about which the Earth revolves [1]. With this formulation, the varying position vector between the Earth and the Sun is specified as $\boldsymbol{d}_e = d_e\hat{\boldsymbol{d}}_e$ and split into a magnitude d_e and direction $\hat{\boldsymbol{d}}_e$, both of which are functions of the Earth true anomaly ν

$$d_e = \frac{P}{1 + E\cos\nu} \tag{1}$$

$$\hat{\boldsymbol{d}}_e = \cos\nu\hat{\boldsymbol{E}}_e + \sin\nu\hat{\boldsymbol{E}}_{e_\perp} \tag{2}$$

where P and E are the orbit parameter and eccentricity of the Earth's heliocentric orbit, respectively.

The Moon's actual motion is very complex; high-precision lunar ephemerides are available through the Jet Propulsion Laboratory, which account for the relativistic n-body equations of motion for the point-mass Sun, Moon, planets, and major asteroids, perturbations on the orbit of the Earth-Moon barycenter from the interaction of the point-mass Sun with the figure, solid-body tides of both the Earth and Moon, and observations of lunar laser ranging.[6] Our purpose in this paper is to adopt the simplest possible expressions useful for studying the long-term evolution of HAMR debris orbits. These expressions must reveal the qualitative regularities of motion, and they must provide, with a certain degree of accuracy, a way of obtaining quantitative predictions of long-term changes. To that end, we assume the Moon is on an osculating elliptical orbit in which the lunar node precesses clockwise in the ecliptic plane with a period of about 18.61 years. We define a geocentric orbit frame, $(\hat{\boldsymbol{E}}_m, \hat{\boldsymbol{E}}_{m_\perp}, \hat{\boldsymbol{H}}_m)$, where $\hat{\boldsymbol{E}}_m$ is the unit vector pointing to the orbit perigee, $\hat{\boldsymbol{E}}_{m_\perp} = \hat{\boldsymbol{H}}_m \times \hat{\boldsymbol{E}}_m$, and $\hat{\boldsymbol{H}}_m$ is the Moon's angular momentum unit vector, about which the Moon revolves. These vectors are resolved using the Moon's ecliptic orbital elements in which $\Omega_m(t) = \Omega_{m_0} + \dot{\Omega}_m(t - t_0)$, where $\dot{\Omega}_m = -2\pi/P_{\text{sidereal}}$ and P_{sidereal} is the sidereal period of nodal regression in seconds. The position vector from the Earth to the Moon is then be specified as $\boldsymbol{d}_m = d_m\hat{\boldsymbol{d}}_m$, where d_m and $\hat{\boldsymbol{d}}_m$ are given by Eqs. 1 and 2, respectively, using the Moon's orbit parameters.

B. Solar Radiation Pressure

Solar radiation pressure is the largest non-gravitational perturbative force to affect the motion of HAMR objects in high-Earth orbits, causing extreme variations in their orbital parameters over short time periods. Typical analysis of long-term orbit dynamics models the SRP acceleration using the cannonball model, which treats the object as a sphere with constant optical properties.[1,21,24] The total momentum transfer from the incident solar photons is modeled as insolation plus reflection, and the force generated is independent of the body's attitude. Any force component normal to the Sun-line that results from an aspherical shape or nonuniformly reflecting surface is thereby neglected. Then the net acceleration will act in the direction directly away from the Sun-line and have the general form[20]

$$\boldsymbol{a}_{srp} = -(1+\rho)(A/m)P_\Phi\frac{(\boldsymbol{d}_s - \boldsymbol{r})}{|\boldsymbol{d}_s - \boldsymbol{r}|^3} \tag{3}$$

$$= -\beta\frac{(\boldsymbol{d}_s - \boldsymbol{r})}{|\boldsymbol{d}_s - \boldsymbol{r}|^3} \tag{4}$$

where ρ is the reflectance, A/m is the appropriate cross-sectional area-to-mass ratio in m^2/kg, P_Φ is the solar radiation constant and is approximately equal to 1×10^8 kg $\text{km}^3/\text{s}^2/\text{m}^2$, and $\beta = (1+\rho)(A/m)P_\Phi$. The vector from the Earth to the Sun is given by $\boldsymbol{d}_s = -\boldsymbol{d}_e$, and the position vector of the orbiter relative to the Earth is $\boldsymbol{r}$. This solar radiation pressure model can be rewritten as a potential

$$\mathcal{R}_{srp} = -\beta\frac{1}{|\boldsymbol{d}_s - \boldsymbol{r}|} \tag{5}$$

where $\boldsymbol{a}_{srp} = \partial\mathcal{R}_{srp}/\partial\boldsymbol{r}$. If the object is close to the Earth, or $r \ll d_s$, the potential can be further simplified by expanding $1/|\boldsymbol{d}_s - \boldsymbol{r}|$ and keeping the first term that contains the position vector $\boldsymbol{r}$.

$$\mathcal{R}_{srp} = -\frac{\beta}{d_s^3}\boldsymbol{d}_s \cdot \boldsymbol{r} \tag{6}$$

[1]These are the defining orientation integrals of the two-body problem, and can be specified using the classical orbital elements relative to an inertial frame.[20]

with the gradient giving a solar radiation pressure acceleration independent of the object's position relative to the Earth

$$\boldsymbol{a}_{srp} = -\frac{\beta}{d_s^2}\hat{\boldsymbol{d}}_s \tag{7}$$

For a given semi-major axis, reflectivity and A/m value, we define the SRP perturbation angle (first defined by Mignard and Hénon (1984)[15]) as

$$\tan\Lambda = \frac{3\beta}{2}\sqrt{\frac{a}{\mu\mu_s P}} \tag{8}$$

where μ and μ_s are the gravitational parameters of the Earth and the Sun, respectively. We note that as the SRP perturbation becomes strong, $\Lambda \to \pi/2$, and as it becomes weak, $\Lambda \to 0$. The angle Λ can be used to rigorously characterize the strength of the SRP perturbation acting on a body as a function of both its orbit and its non-gravitational parameter. As it combines these two quantities into a single parameter, which completely defines the long-term SRP-only solution (c.f.,[19,21]), we find it efficacious to use as the fundamental, defining characteristic of HAMR objects.

Although the cannonball model captures the general nature of SRP, it does not provide a precise prediction of how an individual object will evolve. However, this simple model is commonly used in the propagation of HAMR debris orbits since there is no method to incorporate a physically realistic SRP model with a lack of a priori information (i.e., object geometry, attitude behavior, surface properties, optical and thermal characteristics, etc.). In Ref. 21, it is explicitly shown that averaging a general SRP force expression in time for a randomly tumbling body, i.e., one that presents all attitudes to space with equal probability, yields precisely the cannonball model. Thus, at this limit, we view the cannonball model as representing an average result. These more general models were investigated in Ref. 18. In the current paper, we will focus on the cannonball model as that will allow a direct comparison with earlier analyses of HAMR debris orbit dynamics (cf.,[1,5,24]).

C. Earth Mass Distribution

We consider the effects of the C_{20} and C_{22} terms of the harmonic expansion of Earth's gravitational potential, which account for the polar and equatorial flattening of the Earth's figure. Inclusion of the dominant zonal and sectoral harmonics is sufficient to capture the main effects of nonsphericity in the Earth's mass distribution at high-altitude orbits. The standard way to represent the potential function of the second degree and order gravity field perturbation is using a body-fixed frame with latitude angle δ measured from the equatorial plane and longitude angle λ measured in the equator from the axis of minimum moment of inertia

$$\mathcal{R}_2 = -\frac{\mu C_{20}}{2r^3}\left(1 - 3\sin^2\delta\right) + \frac{3\mu C_{22}}{r^3}\cos^2\delta\cos 2\lambda \tag{9}$$

where $C_{20} = -J_2$ is the oblateness gravity field coefficient and C_{22} is the ellipticity gravity field coefficient. We state the perturbation function in a general vector expression

$$\mathcal{R}_2 = -\frac{\mu C_{20}}{2r^3}\left[1 - 3(\hat{\boldsymbol{r}}\cdot\hat{\boldsymbol{p}})^2\right] + \frac{3\mu C_{22}}{r^3}\left[(\hat{\boldsymbol{r}}\cdot\hat{\boldsymbol{s}})^2 - (\hat{\boldsymbol{r}}\cdot\hat{\boldsymbol{q}})^2\right] \tag{10}$$

where we assume that the unit vectors $\hat{\boldsymbol{p}}$, $\hat{\boldsymbol{q}}$, and $\hat{\boldsymbol{s}}$ are aligned with the body's maximum, intermediate, and minimum axes of inertia. The perturbing acceleration is then computed as

$$\boldsymbol{a}_2 = \frac{\partial\mathcal{R}_2}{\partial\boldsymbol{r}} \tag{11}$$

$$= \frac{3\mu C_{20}}{2r^4}\left\{\left[1 - 5(\hat{\boldsymbol{r}}\cdot\hat{\boldsymbol{p}})^2\right]\hat{\boldsymbol{r}} + 2(\hat{\boldsymbol{r}}\cdot\hat{\boldsymbol{p}})\hat{\boldsymbol{p}}\right\} - \frac{3\mu C_{22}}{r^4}\left\{5\left[(\hat{\boldsymbol{r}}\cdot\hat{\boldsymbol{s}})^2 - (\hat{\boldsymbol{r}}\cdot\hat{\boldsymbol{q}})^2\right]\hat{\boldsymbol{r}} - 2\left[(\hat{\boldsymbol{r}}\cdot\hat{\boldsymbol{s}})\hat{\boldsymbol{s}} - (\hat{\boldsymbol{r}}\cdot\hat{\boldsymbol{q}})\hat{\boldsymbol{q}}\right]\right\} \tag{12}$$

D. Lunisolar Gravitational Attraction

Also necessary to incorporate in this analysis is the perturbation of the Sun and Moon's gravity on the motion of the HAMR object. These can be modeled as third-body perturbations, and their functional form can be simplified by performing an appropriate expansion. Taking Earth as the center of our dynamical system, the perturbation acceleration from a body with gravitational parameter μ_p is represented as[20]

$$\boldsymbol{a}_p = -\mu_p\left[\frac{\boldsymbol{r} - \boldsymbol{d}_p}{|\boldsymbol{r} - \boldsymbol{d}_p|^3} + \frac{\boldsymbol{d}_p}{|\boldsymbol{d}_p|^3}\right] \tag{13}$$

where $\boldsymbol{d}_p$ is the position vector of the body relative to Earth. For use in perturbation analysis it is convenient to recast this as a perturbing acceleration potential

$$\mathcal{R}_p = \mu_p \left[\frac{1}{|\boldsymbol{r} - \boldsymbol{d}_p|} - \frac{\boldsymbol{d}_p \cdot \boldsymbol{r}}{|\boldsymbol{d}_p|^3} \right] \tag{14}$$

where $\boldsymbol{a}_p = \partial \mathcal{R}_p / \partial \boldsymbol{r}$. As the orbiter's distance from the Earth is small compared to the distance between the Earth and the third body, or $\boldsymbol{r}/\boldsymbol{d}_p \ll 1$, the perturbing potential can be represented as an infinite series using the Legendre expansion resulting in[20]

$$\mathcal{R}_p = \frac{\mu_p}{d_p} \left[\sum_{i=0}^{\infty} \left(\frac{r}{d_p} \right)^i P_{i,0} \left(\frac{\boldsymbol{r} \cdot \boldsymbol{d}_p}{r d_p} \right) - \frac{\boldsymbol{d}_p \cdot \boldsymbol{r}}{d_p^2} \right] \tag{15}$$

Keeping only the first non-constant term, with the Legendre polynomial $P_{2,0}(x) = 1/2(3x^2 - 1)$, yields

$$\mathcal{R}_p = \frac{\mu_p}{2 d_p^3} \left[3(\boldsymbol{r} \cdot \hat{\boldsymbol{d}}_p)^2 - r^2 \right] \tag{16}$$

Thus, to lowest order, the gravitational attraction of the Sun and the Moon is represented as a quadratic form, which is the fundamental approximation made in the Hill problem.[20] Under this approximation the perturbing acceleration simplifies to

$$\boldsymbol{a}_p = \frac{\mu_p}{d_p^3} \left[3(\boldsymbol{r} \cdot \hat{\boldsymbol{d}}_p) \hat{\boldsymbol{d}}_p - \boldsymbol{r} \right] \tag{17}$$

E. Non-averaged Equations of Motion

Combining the above force models, we can define the equations of motion for a HAMR object in orbit about the Earth. In an inertially fixed frame centered at the Earth, they can be stated in relative form

$$\ddot{\boldsymbol{r}} = \frac{\partial U}{\partial \boldsymbol{r}} \tag{18}$$

$$U(\boldsymbol{r}) = \frac{\mu}{r} + \mathcal{R}_{srp}(\boldsymbol{r}) + \mathcal{R}_2(\boldsymbol{r}) + \mathcal{R}_s(\boldsymbol{r}) + \mathcal{R}_m(\boldsymbol{r}) \tag{19}$$

where $\mathcal{R}_s$ and $\mathcal{R}_m$ are third-body acceleration potential functions for the Sun and the Moon, respectively. Performing the partial derivatives, we can state the problem in terms of the perturbation accelerations as

$$\ddot{\boldsymbol{r}} = -\frac{\mu}{r^3} \boldsymbol{r} + \boldsymbol{a}_{srp} + \boldsymbol{a}_2 + \boldsymbol{a}_s + \boldsymbol{a}_m \tag{20}$$

III. Averaged Equations of Motion

We now introduce the concept of averaging as this allows us to evaluate the secular effects of the perturbations on our system. For averaging to be valid, we assume that the perturbing forces are sufficiently small so that, over one orbital period, the deviations of the true trajectory from the Keplerian trajectory are relatively small. In this case, oscillations in the orbital elements will average out over reasonably small periods. We refer the reader to Ref. 2 for a complete description of the mathematical bases of averaging.

Instead of using the classical orbital elements for our perturbation theory, we use the eccentricity vector $\boldsymbol{e}$ and the angular momentum vector normalized by $\sqrt{\mu a}$, denoted as $\boldsymbol{h}$, as the osculating orbital elements for the Gauss perturbation equations. This formulation, first purposed by Richter and Keller (1995),[17] has the significant advantage in being well-defined for all orbits and results in simpler variational equations. Note that $\boldsymbol{e} \cdot \boldsymbol{h} = 0$ and we have the constraint on these elements $\boldsymbol{e} \cdot \boldsymbol{e} + \boldsymbol{h} \cdot \boldsymbol{h} = 1$. We recall that these elements are functions of the classical elements e, i, ω, and Ω, and thus can be used to evaluate their secular rates. Specifically, $\boldsymbol{h} = \sqrt{1 - e^2} \hat{\boldsymbol{h}}$ and $\boldsymbol{e} = e \hat{\boldsymbol{e}}$, where $\hat{\boldsymbol{h}}$ and $\hat{\boldsymbol{e}}$ are given in Appendix A..

We can write these vectors in terms of the position $\boldsymbol{r}$ and velocity $\boldsymbol{v}$ of the orbiter in dyadic notation as

$$\boldsymbol{h} = \frac{1}{\sqrt{\mu a}} \tilde{\boldsymbol{r}} \cdot \boldsymbol{v} \tag{21}$$

$$\begin{aligned} \boldsymbol{e} &= \frac{1}{\mu} \tilde{\boldsymbol{v}} \cdot \tilde{\boldsymbol{r}} \cdot \boldsymbol{v} - \frac{\boldsymbol{r}}{|\boldsymbol{r}|} \\ &= \frac{1}{\mu} \left[r \boldsymbol{v} - (\boldsymbol{r} \cdot \boldsymbol{v}) \boldsymbol{U} \right] \cdot \boldsymbol{v} - \hat{\boldsymbol{r}} \end{aligned} \tag{22}$$

where $\boldsymbol{U}$ is the identity dyad. Differentiating with respect to time, we obtain the Gauss equations for $\boldsymbol{h}$ and $\boldsymbol{e}$:

$$\begin{aligned}\dot{\boldsymbol{h}} &= \frac{\partial \boldsymbol{h}}{\partial \boldsymbol{v}} \cdot \boldsymbol{a}_d \\ &= \frac{1}{\sqrt{\mu a}} \tilde{\boldsymbol{r}} \cdot \boldsymbol{a}_d \end{aligned} \tag{23}$$

$$\begin{aligned}\dot{\boldsymbol{e}} &= \frac{\partial \boldsymbol{e}}{\partial \boldsymbol{v}} \cdot \boldsymbol{a}_d \\ &= \frac{1}{\mu}\left[-\widetilde{\boldsymbol{r} \times \boldsymbol{v}} + \tilde{\boldsymbol{v}} \cdot \tilde{\boldsymbol{r}}\right] \cdot \boldsymbol{a}_d \\ &= \frac{1}{\mu}\left(-\sqrt{\mu a}\tilde{\boldsymbol{h}} + \tilde{\boldsymbol{v}} \cdot \tilde{\boldsymbol{r}}\right) \cdot \boldsymbol{a}_d \end{aligned} \tag{24}$$

where $\boldsymbol{a}_d$ is an arbitrary disturbing acceleration.

Averaging is defined as an operator that computes the time average of a quantity over one orbit period, while keeping all other orbital elements constant.[20] Thus, the averaged equations of motion are defined by

$$\bar{\dot{\boldsymbol{h}}} = \frac{1}{2\pi}\int_0^{2\pi} \dot{\boldsymbol{h}}\, \mathrm{d}M \tag{25}$$

$$\bar{\dot{\boldsymbol{e}}} = \frac{1}{2\pi}\int_0^{2\pi} \dot{\boldsymbol{e}}\, \mathrm{d}M \tag{26}$$

where the over bar indicates the averaged value, the averaging is carried out over the orbiter's unpreturbed two-body motion about the Earth, and M is the orbiter's mean anomaly. Since the perturbations in our system each come from a potential, the semi-major axis becomes a constant of the motion, and is thus treated as a free parameter in our solutions.

A. Averaged SRP Dynamics

Substituting the perturbation acceleration, Eq. 7, into Eqs. 23 and 24, the differential equations for $\boldsymbol{h}$ and $\boldsymbol{e}$, resulting from SRP acceleration, can be written as

$$\begin{aligned}\dot{\boldsymbol{h}}_{srp} &= \frac{1}{\sqrt{\mu a}} \tilde{\boldsymbol{r}} \cdot \left(-\frac{\beta}{d_s^2}\hat{\boldsymbol{d}}_s\right) \\ &= \frac{\beta}{\sqrt{\mu a} d_s^2} \tilde{\hat{\boldsymbol{d}}}_s \cdot \boldsymbol{r} \end{aligned} \tag{27}$$

$$\begin{aligned}\dot{\boldsymbol{e}}_{srp} &= \frac{1}{\mu}\left(-\sqrt{\mu a}\tilde{\boldsymbol{h}} + \tilde{\boldsymbol{v}} \cdot \tilde{\boldsymbol{r}}\right) \cdot \left(-\frac{\beta}{d_s^2}\hat{\boldsymbol{d}}_s\right) \\ &= -\frac{\beta}{\mu d_s^2}\left(\sqrt{\mu a}\tilde{\hat{\boldsymbol{d}}}_s \cdot \boldsymbol{h} + \tilde{\boldsymbol{v}} \cdot \tilde{\boldsymbol{r}} \cdot \hat{\boldsymbol{d}}_s\right) \end{aligned} \tag{28}$$

Averaging over these equations, we find[2]

$$\bar{\dot{\boldsymbol{h}}}_{srp} = \frac{\beta}{\sqrt{\mu a} d_s^2} \tilde{\hat{\boldsymbol{d}}}_s \cdot \bar{\boldsymbol{r}} \tag{29}$$

$$\bar{\dot{\boldsymbol{e}}}_{srp} = -\frac{\beta}{\mu d_s^2}\left(\sqrt{\mu a}\tilde{\hat{\boldsymbol{d}}}_s \cdot \boldsymbol{h} + \overline{\tilde{\boldsymbol{v}} \cdot \tilde{\boldsymbol{r}}} \cdot \hat{\boldsymbol{d}}_s\right) \tag{30}$$

in which we note[20]

$$\bar{\boldsymbol{r}} = -\frac{3}{2} a \boldsymbol{e} \tag{31}$$

$$\begin{aligned}\overline{\tilde{\boldsymbol{v}} \cdot \tilde{\boldsymbol{r}}} &= \overline{\boldsymbol{r}\boldsymbol{v}} - (\overline{\boldsymbol{r} \cdot \boldsymbol{v}})\boldsymbol{U} \\ &= -\frac{1}{2}\sqrt{\mu a}\tilde{\boldsymbol{h}} \end{aligned} \tag{32}$$

[2]The bar ($\bar{-}$) operator is omitted from the Keplerian elements in what follows because there is no ambiguity; i.e., all variables are averaged variables.

Consequently,

$$\bar{\dot{\boldsymbol{h}}}_{srp} = -\frac{3}{2}\sqrt{\frac{a}{\mu}}\frac{\beta}{d_s^2}\tilde{\hat{\boldsymbol{d}}}_s \cdot \boldsymbol{e} \tag{33}$$

$$\bar{\dot{\boldsymbol{e}}}_{srp} = -\frac{3}{2}\sqrt{\frac{a}{\mu}}\frac{\beta}{d_s^2}\tilde{\hat{\boldsymbol{d}}}_s \cdot \boldsymbol{h} \tag{34}$$

In Ref. 19, Scheeres showed that the averaged Gauss equations, Eqs. 33 and 34, can be solved in closed form, yielding an analytical solution for the secular variation in the eccentricity and angular momentum vectors. The analytical solution is expressed in a frame that rotates with the Sun-line, and solutions are periodic in $\nu/\cos\Lambda$, repeating every Earth true anomaly $2\pi\cos\Lambda$. Thus, over one heliocentric orbit the solution will advance $1/\cos\Lambda$ times. As the perturbation grows large, and Λ approaches $\pi/2$, the solution will repeat many times over one year. Conversely, as the perturbation grows small the solution will repeat only once every year. Since the solutions are time-periodic, performing a second average of the Gauss equations over the motion of the Sun results in the SRP perturbations averaging to zero. Thus, unlike third-body perturbations, a doubly-averaged SRP formulation is inappropriate.

In a previous study,[21] we applied the SRP-only averaged solution to the dynamics of HAMR objects in GEO and GPS orbit regimes having a variety of Λ values. One of the surprising aspects of the theory is that the extremely simple, periodic behavior that occurs relative to the Earth-Sun rotating frame becomes quite complex and aperiodic in the Earth equatorial frame. The presence of the complex oscillations in eccentricity and inclination, with short-period and long-period terms, is just an artifact of transforming into the Earth equatorial frame.

B. Averaged J_2 Dynamics

Hu and Scheeres (2002)[8] study the secular motion about slowly rotating asteroids in a second degree and order gravity field. We note that in general, the orbital elements will have periodic motion resulting from the C_{22} dynamics, and thus these effects, if they exist, will get averaged out over longer time periods. For HAMR objects in GEO space, Lemaître *et al.* (2009)[10] found that a resonance occurs from the C_{22} dynamics, giving rise to chaotic behavior localized to a narrow range of semi-major axis. With mean motion averaging, our theory will be unable to account for this subtle, and potentially important, aspect of motion. Therefore, we only consider the averaged C_{20} dynamics in our system. The secular Gauss equations, resulting from Earth oblateness perturbations, were derived previously[18] and are given below:

$$\dot{\boldsymbol{h}}_{20} = \frac{3nC_{20}}{2a^2h^5}(\boldsymbol{h}\cdot\hat{\boldsymbol{p}})\tilde{\hat{\boldsymbol{p}}}\cdot\boldsymbol{h} \tag{35}$$

$$\dot{\boldsymbol{e}}_{20} = \frac{3nC_{20}}{4a^2h^5}\left[\left(1-\frac{5}{h^2}(\boldsymbol{h}\cdot\hat{\boldsymbol{p}})^2\right)\tilde{\boldsymbol{h}} + 2(\boldsymbol{h}\cdot\hat{\boldsymbol{p}})\tilde{\hat{\boldsymbol{p}}}\right]\cdot\boldsymbol{e} \tag{36}$$

C. Averaged Third-body Dynamics

Singly-averaged Equations : Substituting the third-body perturbation gravitational acceleration, Eq. 17, into Eqs. 23, the differential equation for $\boldsymbol{h}$ can be written as

$$\begin{aligned}\dot{\boldsymbol{h}}_p &= \frac{1}{\sqrt{\mu a}}\tilde{\boldsymbol{r}}\cdot\left\{\frac{\mu_p}{d_p^3}\left[3(\boldsymbol{r}\cdot\hat{\boldsymbol{d}}_p)\hat{\boldsymbol{d}}_p - \boldsymbol{r}\right]\right\}\\ &= \frac{3\mu_p}{\sqrt{\mu a}d_p^3}\hat{\boldsymbol{d}}_p\cdot\boldsymbol{r}\boldsymbol{r}\cdot\tilde{\hat{\boldsymbol{d}}}_p\end{aligned} \tag{37}$$

We now average over the orbiter's unpreturbed two-body motion about the Earth

$$\bar{\dot{\boldsymbol{h}}}_p = \frac{3\mu_p}{\sqrt{\mu a}d_p^3}\hat{\boldsymbol{d}}_p\cdot\overline{\boldsymbol{r}\boldsymbol{r}}\cdot\tilde{\hat{\boldsymbol{d}}}_p \tag{38}$$

in which we note[20]

$$\begin{aligned}\overline{\boldsymbol{r}\boldsymbol{r}} &= \frac{1}{2}a^2\left[(1+4e^2)\hat{\boldsymbol{e}}\hat{\boldsymbol{e}} + (1-e^2)\hat{\boldsymbol{e}}_\perp\hat{\boldsymbol{e}}_\perp\right]\\ &= \frac{1}{2}a^2\left[(1-e^2)\boldsymbol{U} + 5\boldsymbol{e}\boldsymbol{e} - \boldsymbol{h}\boldsymbol{h}\right]\end{aligned} \tag{39}$$

Consequently,

$$\begin{aligned}\bar{\dot{\boldsymbol{h}}}_p &= \frac{3\mu_p}{\sqrt{\mu a}d_p^3}\hat{\boldsymbol{d}}_p \cdot \left\{\frac{1}{2}a^2\left[(1-e^2)\boldsymbol{U} + 5\boldsymbol{ee} - \boldsymbol{hh}\right]\right\} \cdot \bar{\tilde{\boldsymbol{d}}}_p \\ &= \frac{3\mu_p}{2nd_p^3}\hat{\boldsymbol{d}}_p \cdot [5\boldsymbol{ee} - \boldsymbol{hh}] \cdot \bar{\tilde{\boldsymbol{d}}}_p \end{aligned} \tag{40}$$

Substituting the perturbation acceleration into Eq. 24, the differential equation for $\boldsymbol{e}$ can be written as

$$\begin{aligned}\dot{\boldsymbol{e}}_p &= \frac{1}{\mu}\left[-\sqrt{\mu a}\tilde{\boldsymbol{h}} + \tilde{\boldsymbol{v}}\cdot\tilde{\boldsymbol{r}}\right]\cdot\left\{\frac{\mu_p}{d_p^3}\left[3(\boldsymbol{r}\cdot\hat{\boldsymbol{d}}_p)\hat{\boldsymbol{d}}_p - \boldsymbol{r}\right]\right\} \\ &= \frac{\mu_p}{\mu d_p^3}\left\{-3\sqrt{\mu a}(\boldsymbol{r}\cdot\hat{\boldsymbol{d}}_p)\tilde{\boldsymbol{h}}\cdot\hat{\boldsymbol{d}}_p + \sqrt{\mu a}\tilde{\boldsymbol{h}}\cdot\boldsymbol{r} + 3(\boldsymbol{r}\cdot\hat{\boldsymbol{d}}_p)\tilde{\boldsymbol{v}}\cdot\tilde{\boldsymbol{r}}\cdot\hat{\boldsymbol{d}}_p\right\} \\ &= \frac{\mu_p}{\mu d_p^3}\left\{-3\sqrt{\mu a}(\boldsymbol{r}\cdot\hat{\boldsymbol{d}}_p)\tilde{\boldsymbol{h}}\cdot\hat{\boldsymbol{d}}_p + \sqrt{\mu a}\tilde{\boldsymbol{h}}\cdot\boldsymbol{r} + 3\hat{\boldsymbol{d}}_p\cdot[\boldsymbol{rrv} - (\boldsymbol{r}\cdot\boldsymbol{v})\boldsymbol{rU}]\cdot\hat{\boldsymbol{d}}_p\right\}\end{aligned} \tag{41}$$

Averaging over this equation, we find

$$\bar{\dot{\boldsymbol{e}}}_p = \frac{\mu_p}{\mu d_p^3}\left\{-3\sqrt{\mu a}(\bar{\boldsymbol{r}}\cdot\hat{\boldsymbol{d}}_p)\tilde{\boldsymbol{h}}\cdot\hat{\boldsymbol{d}}_p + \sqrt{\mu a}\tilde{\boldsymbol{h}}\cdot\bar{\boldsymbol{r}} + 3\hat{\boldsymbol{d}}_p\cdot\left[\overline{\boldsymbol{rrv}} - \overline{(\boldsymbol{r}\cdot\boldsymbol{v})\boldsymbol{r}}\boldsymbol{U}\right]\cdot\hat{\boldsymbol{d}}_p\right\} \tag{42}$$

where (cf., Appendix B.)

$$\overline{(\boldsymbol{r}\cdot\boldsymbol{v})\boldsymbol{r}} = \frac{1}{2}\sqrt{\mu}a^{3/2}e\sqrt{1-e^2}\hat{\boldsymbol{e}}_\perp \tag{43}$$

$$\overline{\boldsymbol{rrv}} = \frac{1}{2}\sqrt{\mu}a^{3/2}e\sqrt{1-e^2}(-2\hat{\boldsymbol{e}}\hat{\boldsymbol{e}}\hat{\boldsymbol{e}}_\perp + \hat{\boldsymbol{e}}\hat{\boldsymbol{e}}_\perp\hat{\boldsymbol{e}} + \hat{\boldsymbol{e}}_\perp\hat{\boldsymbol{e}}\hat{\boldsymbol{e}}) \tag{44}$$

Consequently,

$$\begin{aligned}\bar{\dot{\boldsymbol{e}}}_p &= \frac{3e\sqrt{1-e^2}\mu_p}{2nd_p^3}\left\{3(\hat{\boldsymbol{e}}\cdot\hat{\boldsymbol{d}}_p)\bar{\tilde{\boldsymbol{h}}}\cdot\hat{\boldsymbol{d}}_p - \bar{\tilde{\boldsymbol{h}}}\cdot\hat{\boldsymbol{e}} + \hat{\boldsymbol{d}}_p\cdot[-2\hat{\boldsymbol{e}}\hat{\boldsymbol{e}}\hat{\boldsymbol{e}}_\perp + \hat{\boldsymbol{e}}\hat{\boldsymbol{e}}_\perp\hat{\boldsymbol{e}} + \hat{\boldsymbol{e}}_\perp\hat{\boldsymbol{e}}\hat{\boldsymbol{e}} - \hat{\boldsymbol{e}}_\perp\boldsymbol{U}]\cdot\hat{\boldsymbol{d}}_p\right\} \\ &= \frac{3e\sqrt{1-e^2}\mu_p}{2nd_p^3}\left\{3(\hat{\boldsymbol{e}}\cdot\hat{\boldsymbol{d}}_p)\bar{\tilde{\boldsymbol{h}}}\cdot\hat{\boldsymbol{d}}_p - \bar{\tilde{\boldsymbol{h}}}\cdot\hat{\boldsymbol{e}} + (\hat{\boldsymbol{e}}\cdot\hat{\boldsymbol{d}}_p)^2\hat{\boldsymbol{e}}_\perp - (\hat{\boldsymbol{e}}\cdot\hat{\boldsymbol{d}}_p)\hat{\boldsymbol{d}}_p\cdot\bar{\tilde{\boldsymbol{h}}}\cdot\hat{\boldsymbol{e}}\hat{\boldsymbol{e}} - (\hat{\boldsymbol{e}}_\perp\cdot\hat{\boldsymbol{d}}_p)\hat{\boldsymbol{d}}_p\right\} \\ &= \frac{3e\sqrt{1-e^2}\mu_p}{2nd_p^3}\left\{3(\hat{\boldsymbol{e}}\cdot\hat{\boldsymbol{d}}_p)\bar{\tilde{\boldsymbol{h}}}\cdot\hat{\boldsymbol{d}}_p - \bar{\tilde{\boldsymbol{h}}}\cdot\hat{\boldsymbol{e}} + (\hat{\boldsymbol{e}}\cdot\hat{\boldsymbol{d}}_p)^2\hat{\boldsymbol{e}}_\perp - (\hat{\boldsymbol{e}}\cdot\hat{\boldsymbol{d}}_p)\hat{\boldsymbol{d}}_p\cdot\bar{\tilde{\boldsymbol{h}}}\cdot(\boldsymbol{U} - \hat{\boldsymbol{e}}_\perp\hat{\boldsymbol{e}}_\perp - \hat{\boldsymbol{h}}\hat{\boldsymbol{h}}) - \hat{\boldsymbol{e}}_\perp\cdot\hat{\boldsymbol{d}}_p\hat{\boldsymbol{d}}_p\right\} \\ &= \frac{3e\sqrt{1-e^2}\mu_p}{2nd_p^3}\left\{4(\hat{\boldsymbol{e}}\cdot\hat{\boldsymbol{d}}_p)\bar{\tilde{\boldsymbol{h}}}\cdot\hat{\boldsymbol{d}}_p - \bar{\tilde{\boldsymbol{h}}}\cdot\hat{\boldsymbol{e}} - \hat{\boldsymbol{e}}_\perp\cdot\hat{\boldsymbol{d}}_p\hat{\boldsymbol{d}}_p\right\} \\ &= \frac{3\mu_p}{2nd_p^3}\left\{4(\boldsymbol{e}\cdot\hat{\boldsymbol{d}}_p)\tilde{\boldsymbol{h}}\cdot\hat{\boldsymbol{d}}_p - \tilde{\boldsymbol{h}}\cdot\boldsymbol{e} - \hat{\boldsymbol{d}}_p\hat{\boldsymbol{d}}_p\cdot\tilde{\boldsymbol{h}}\cdot\boldsymbol{e}\right\}\end{aligned} \tag{45}$$

We note that the singly-averaged Gauss equations, Eqs. 40 and 45, contain no singularities; that is, they are valid for all eccentricity and all inclination. In addition, since we make no assumptions on the motion of the disturbing body, except that its position is fixed during the process of averaging, it is possible to use a high-accuracy ephemeris for $\hat{\boldsymbol{d}}_p$.

Doubly-averaged Equations : The singly-averaged Gauss equations can be restated as

$$\bar{\dot{\boldsymbol{h}}}_p = \frac{3\mu_p}{2n}\left[-5\boldsymbol{e}\cdot\frac{\hat{\boldsymbol{d}}_p\hat{\boldsymbol{d}}_p}{d_p^3}\cdot\bar{\tilde{\boldsymbol{e}}} + \boldsymbol{h}\cdot\frac{\hat{\boldsymbol{d}}_p\hat{\boldsymbol{d}}_p}{d_p^3}\cdot\bar{\tilde{\boldsymbol{h}}}\right] \tag{46}$$

$$\bar{\dot{\boldsymbol{e}}}_p = \frac{3\mu_p}{2n}\left\{-4\boldsymbol{e}\cdot\frac{\hat{\boldsymbol{d}}_p\hat{\boldsymbol{d}}_p}{d_p^3}\cdot\bar{\tilde{\boldsymbol{h}}} - \frac{1}{d_p^3}\bar{\tilde{\boldsymbol{h}}}\cdot\boldsymbol{e} - \frac{\hat{\boldsymbol{d}}_p\hat{\boldsymbol{d}}_p}{d_p^3}\cdot\bar{\tilde{\boldsymbol{h}}}\cdot\boldsymbol{e}\right\} \tag{47}$$

in which the disturbing body is now assumed to be in an elliptic orbit.

We now perform a second average over $\hat{\boldsymbol{d}}_p$ as

$$\bar{\bar{\dot{\boldsymbol{h}}}}_p = \frac{1}{2\pi}\int_0^{2\pi} \bar{\dot{\boldsymbol{h}}}\,\mathrm{d}M_p \tag{48}$$

$$= \frac{3\mu_p}{2n}\left[-5\boldsymbol{e}\cdot\overline{\left(\frac{\hat{\boldsymbol{d}}_p\hat{\boldsymbol{d}}_p}{d_p^3}\right)}\cdot\tilde{\boldsymbol{e}} + \boldsymbol{h}\cdot\overline{\left(\frac{\hat{\boldsymbol{d}}_p\hat{\boldsymbol{d}}_p}{d_p^3}\right)}\cdot\tilde{\boldsymbol{h}}\right] \tag{49}$$

$$\bar{\bar{\dot{\boldsymbol{e}}}}_p = \frac{1}{2\pi}\int_0^{2\pi} \bar{\dot{\boldsymbol{e}}}\,\mathrm{d}M_p \tag{50}$$

$$= \frac{3\mu_p}{2n}\left\{-4\boldsymbol{e}\cdot\overline{\left(\frac{\hat{\boldsymbol{d}}_p\hat{\boldsymbol{d}}_p}{d_p^3}\right)}\cdot\tilde{\boldsymbol{h}} - \overline{\left(\frac{1}{d_p^3}\right)}\tilde{\boldsymbol{h}}\cdot\boldsymbol{e} - \overline{\left(\frac{\hat{\boldsymbol{d}}_p\hat{\boldsymbol{d}}_p}{d_p^3}\right)}\cdot\tilde{\boldsymbol{h}}\cdot\boldsymbol{e}\right\} \tag{51}$$

where (=) denotes the double averaged value. Note that[20]

$$\overline{\left(\frac{\hat{\boldsymbol{d}}_p\hat{\boldsymbol{d}}_p}{d_p^3}\right)} = \frac{1}{2a_p^3(1-e_p^2)^{3/2}}\left(\boldsymbol{U} - \hat{\boldsymbol{H}}_p\hat{\boldsymbol{H}}_p\right) \tag{52}$$

$$\overline{\left(\frac{1}{d_p^3}\right)} = \frac{1}{a_p^3(1-e_p^2)^{3/2}} \tag{53}$$

where $\hat{\boldsymbol{H}}_p$ is angular momentum unit vector of the perturbing body. Consequently, the doubly-averaged third-body dynamics for an elliptically orbiting disturbing body become

$$\bar{\bar{\dot{\boldsymbol{h}}}}_p = \frac{3\mu_p}{4na_p^3(1-e_p^2)^{3/2}}\left[-5\boldsymbol{e}\cdot\left(\boldsymbol{U} - \hat{\boldsymbol{H}}_p\hat{\boldsymbol{H}}_p\right)\cdot\tilde{\boldsymbol{e}} + \boldsymbol{h}\cdot\left(\boldsymbol{U} - \hat{\boldsymbol{H}}_p\hat{\boldsymbol{H}}_p\right)\cdot\tilde{\boldsymbol{h}}\right]$$

$$= -\frac{3\mu_p}{4na_p^3(1-e_p^2)^{3/2}}\hat{\boldsymbol{H}}_p\cdot[5\boldsymbol{e}\boldsymbol{e} - \boldsymbol{h}\boldsymbol{h}]\cdot\tilde{\hat{\boldsymbol{H}}}_p \tag{54}$$

$$\bar{\bar{\dot{\boldsymbol{e}}}}_p = \frac{3\mu_p}{4na_p^3(1-e_p^2)^{3/2}}\left\{-4\boldsymbol{e}\cdot\left(\boldsymbol{U} - \hat{\boldsymbol{H}}_p\hat{\boldsymbol{H}}_p\right)\cdot\tilde{\boldsymbol{h}} - 2\tilde{\boldsymbol{h}}\cdot\boldsymbol{e} - \left(\boldsymbol{U} - \hat{\boldsymbol{H}}_p\hat{\boldsymbol{H}}_p\right)\cdot\tilde{\boldsymbol{h}}\cdot\boldsymbol{e}\right\}$$

$$= -\frac{3\mu_p}{4na_p^3(1-e_p^2)^{3/2}}\left\{4(\boldsymbol{e}\cdot\hat{\boldsymbol{H}}_p)\tilde{\boldsymbol{h}}\cdot\hat{\boldsymbol{H}}_p - \tilde{\boldsymbol{h}}\cdot\boldsymbol{e} - \hat{\boldsymbol{H}}_p\hat{\boldsymbol{H}}_p\cdot\tilde{\boldsymbol{h}}\cdot\boldsymbol{e}\right\} \tag{55}$$

As shown in Appendix C., the secular variations in the classical orbital elements, resulting from the doubly-averaged third-body dynamics, can be formulated in terms of the vectors $\boldsymbol{h}$ and $\boldsymbol{e}$. These orbital rates can also be found by averaging the Hill-approximated third-body perturbing potential (Eq. 16) over the mean motion of the Earth orbiter and the disturbing body, respectively, and then substituting this doubly-averaged potential into the Lagrange planetary equations. This result was originally realized by Lidov (1961),[11] Lorell, and Anderson (1962)[13] in the study of lunar satellite motion. Our unique approach, however, has the advantage that the orbit-averaged equations, given by Eqs. 54 and 55, are completely non-singular and are written in a concise analytical vector form.

D. Secular Gauss Equations

The secular evolution of the normalized angular momentum vector $\boldsymbol{h}$ and the eccentricity vector $\boldsymbol{e}$ in the presence of SRP, J_2 and lunisolar perturbations can be stated as

$$\dot{\boldsymbol{h}} = \dot{\boldsymbol{h}}_{srp} + \dot{\boldsymbol{h}}_{20} + \dot{\boldsymbol{h}}_s + \dot{\boldsymbol{h}}_m \tag{56}$$

$$\dot{\boldsymbol{e}} = \dot{\boldsymbol{e}}_{srp} + \dot{\boldsymbol{e}}_{20} + \dot{\boldsymbol{e}}_s + \dot{\boldsymbol{e}}_m \tag{57}$$

where the over bar has been dropped, the SRP dynamics are given by Eqs. 33 and 34, and the C_{20} dynamics are given by Eqs. 35 and 36. The lunisolar dynamics can either be represented by the singly-averaged equations, Eqs. 40 and 45, or the doubly-averaged equations, Eqs. 54 and 55. In this formulation, the motion of the disturbing bodies can either be supplied from theory, i.e., the two-body solution, or can be provided by an ephemeris.

Combining all of these perturbations leads to a highly-nonlinear system, which does not appear integrable. Although the exact averaged solution is presumably inaccessible, the expressions given in Eqs. 56 and 57 are several

hundred times faster to numerically integrate than their non-averaged Newtonian counterparts. With these results it is possible to predict accurately the long term orbital behavior of HAMR objects, given the initial values of the orbital elements and the initial geometry of the Earth-Moon-Sun system; the latter being important for calculation of Moon-induced perturbations.

IV. Long-term Dynamics of HAMR Objects

Numerical integration of the precise non-averaged equations of motion, Eq. 20, represents the most accurate means of calculating the exact trajectory of an orbiting body in a given time interval. Comparison of these solutions with the results obtained from the averaged formulas is a significantly reliable estimate of the accuracy of the approximated equations. Such comparison permits us to conclude about the applicability of the averaged equations for considering the evolution of HAMR debris orbits. Particular emphasis is given in these applications to HAMR objects with area-to-mass ratios and conditions of those observed in nearly geosynchronous orbit by optical observations.[22] The initial conditions for all objects examined, given in terms of mean Keplerian orbital elements, are provided in Table 1. To give an idea of the main characteristics of motion, the dynamics were simulated using a reflectance value of 0.36, and area-to-mass ratios between 1 and 20 m^2/kg. For a given semi-major axis, reflectivity and A/m value, we compute the corresponding Λ angle which we use to characterize the evolutionary behavior of HAMR debris orbits. The SRP perturbation angles, as computed from Eq. 8, are shown in Table 2.

Table 1: Initial orbital elements for HAMR debris released in near GEO orbit.

Epoch†	a [km]	e	i [°]	Ω [°]	ω [°]	M [°]
1950.01.01 12:00:00 UTC	42164.465	0.0001	0.0971	50.001	220.001	301.221

† The epoch date determines the initial dynamical configuration of the Earth-Moon-Sun system. The orbital elements for the Earth and the Moon, corresponding to this epoch, are taken from the JPL ephemeris.

Table 2: Area-to-mass ratios and corresponding SRP perturbation angles† for GEO objects.

A/m [m^2/kg]	$(1+\rho)(A/m)$ [m^2/kg]	Λ [°]
1	1.36	0.85
5	6.8	4.26
10	13.6	8.47
15	20.4	12.60
20	27.2	16.59

† A reflectance value of 0.36 was assumed.

A. Newtonian Non-averaged Dynamics

In order to better understand the long-term dynamics of the system and to validate our semi-analytical averaged theory, we propagate the orbits for 100 years, using the full non-averaged equations of motion (see Figure 1). For the non-averaged dynamics, we use the high accuracy solar system ephemeris, provided by JPL, to calculate the position vectors of the Sun and the Moon. The long-term eccentricity and inclination evolution shown in Figures 1(a) and 1(b) closely matches the results obtained by Anselmo and Pardini.[1] Concerning the eccentricity evolution, solar radiation pressure alone induces sub-yearly oscillations with period $2\pi\cos\Lambda$; the amplitude increasing with increasing Λ. Inclusion of the C_{20} and C_{22} harmonics causes only slight changes in the short-term oscillations, but induces long-period small fluctuations in the maximum amplitudes. The dynamical coupling between SRP and J_2 becomes more pronounced with increasing Λ (c.f.,[18]). The addition of third-body perturbations, primarily the attraction of the Moon, causes a slight increase in the short-term amplitudes, and gives rise to long-term aperiodic oscillations in the maximum amplitudes. The evolution of the two-dimensional eccentricity vector, $e\left[\cos\omega\cos\Omega - \cos i\sin\omega\sin\Omega; \cos\omega\sin\Omega + \cos i\sin\omega\cos\Omega\right]$, is characterized by both a yearly and long-term regression; the latter exhibiting complex evolutionary behavior (see Figure 1(c)).

Regarding the inclination evolution, solar radiation pressure accounts for the sub-yearly oscillations that ride on top of the longer-term secular drift, and the reduction in the long-term oscillation periods with increasing Λ. The

addition of geopotential harmonics, mainly C_{20}, brings about a reduction in both the amplitude and period of the long-term oscillations. Inclusion of lunisolar perturbations causes a decrease in the long-term oscillation periods, and for certain values of Λ—most notably $\Lambda = 12.60°$—causes large fluctuations (peak-to-peak changes) in the maximum amplitudes. These fluctuations manifest themselves as a beating phenomenon in the evolution of the two-dimensional angular momentum unit vector, $[\sin i \sin\Omega, -\sin i \cos\Omega]$. Note that for lower values of Λ, this complex behavior is not observed, as shown in Figure 1(d).

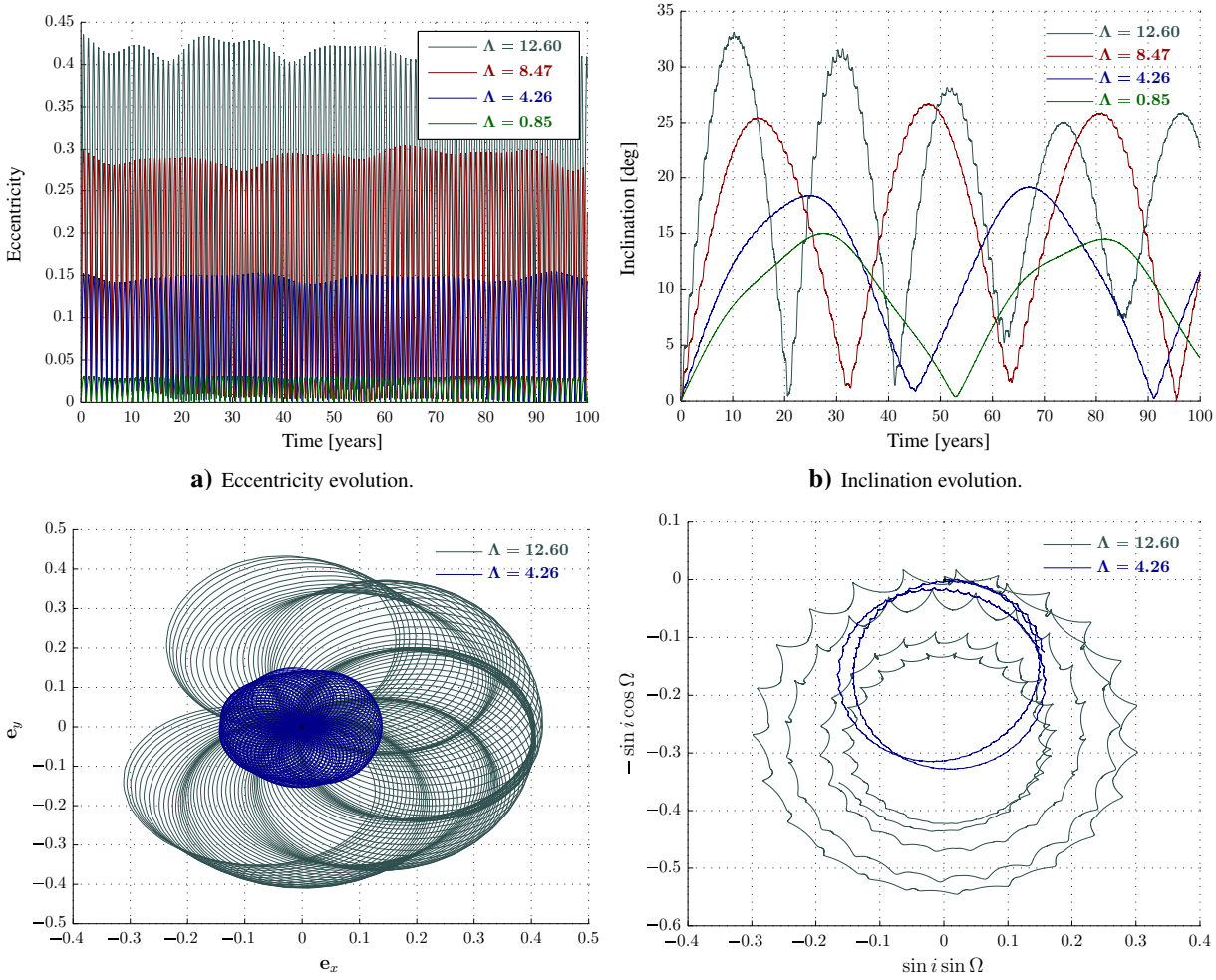

a) Eccentricity evolution.

b) Inclination evolution.

c) Two-dimensional eccentricity vector evolution.

d) Two-dimensional angular momentum unit vector evolution.

Figure 1: Long-term orbit evolution (100 years) in the Earth equatorial frame for different values of the SRP perturbation angle, as predicted by the full non-averaged equations of motion, Eq. 20, using Eq. 4 for SRP, Eq. 12 for C_{20} and C_{22}, and Eq. 13 for lunisolar perturbations. The position vectors of both the Sun and the Moon were computed using the JPL ephemeris.

B. Secular Dynamics

Since our Newtonian non-averaged results compare well, both quantitatively and qualitatively, with those of Anselmo and Pardini[3], they can be used as a logical basis for assessing the validity of our averaged theory. We are particularly interested in distinguishing between cause and effect and in identifying the precise origin of any perturbation experienced by the HAMR object. To that end, we avoid using the precise JPL ephemeris, and instead assume two-body dynamics for the Sun and the Moon, for which the lunar node regresses in the ecliptic plane with a sidereal period of ~ 18.61 years (see Section II. A.).

The orbit evolution of several HAMR objects, obtained using numerical integrations of the singly-averaged equa-

[3]In addition to our force model, they account for higher-order gravity field perturbations and Earth shadow effects in their numerical integrations.

tions of motion, are shown in Figure 2. The approximated averaged equations, using two-body dynamics and accounting for the regression of the Moon's node, gives us nearly identical plots at this level of resolution as the full Newtonian non-averaged simulations, using a precise ephemeris. We do not use any special formalism in our integrations to preserve the constraints on $\boldsymbol{h}$ and $\boldsymbol{e}$[4], yet after 100 years, they are satisfied to over one part per billion.

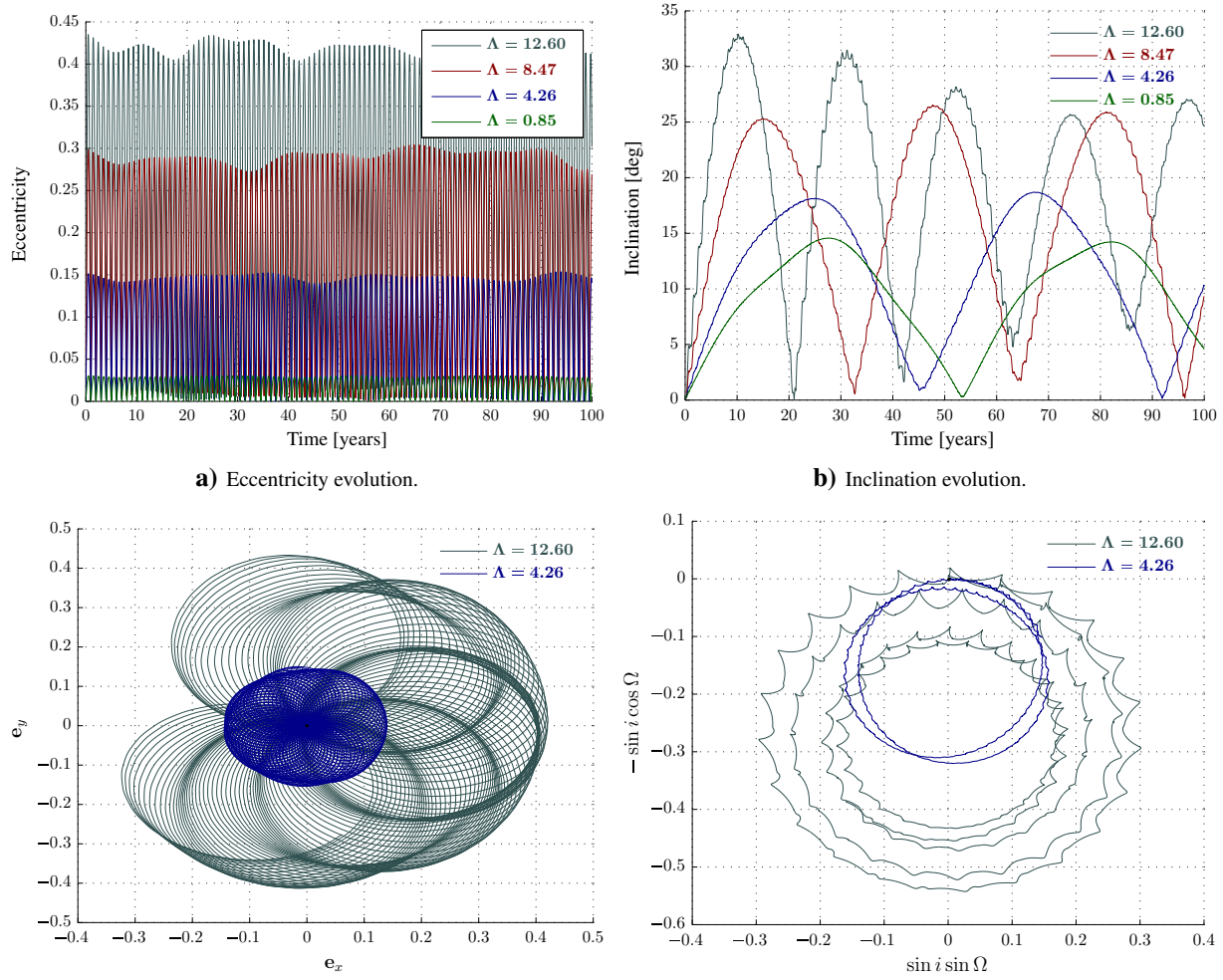

a) Eccentricity evolution.

b) Inclination evolution.

c) Two-dimensional eccentricity vector evolution.

d) Two-dimensional angular momentum unit vector evolution.

Figure 2: Long-term orbit evolution (100 years) in the Earth equatorial frame for different values of the SRP perturbation angle, as predicted by the singly-averaged equations of motion, Eqs. 40 and 45. The position vectors of both the Sun and Moon were computed using two-body dynamics, accounting for lunar nodal regression.

We now illustrate the limitations and domain of validity of the doubly-averaged third-body equations, which, in their Lagrangian form (see Appendix C.), have been used extensively for lunar orbiter long-arc analysis during the 1960s (c.f.,[11,13]). The long-term evolution of the two dimensional angular momentum unit vector and eccentricity vector are shown in Figure 3. Since the doubly-averaged equations, Eqs. 54 and 55, are written in a vector form that depend on the angular momentum unit vector of the perturbing body, $\hat{\boldsymbol{H}}_p$, we can account for the regression of the lunar node in our simulations[5]. In all cases considered, the doubly-averaged equations predict the qualitative nature of the orbits; however, the angular momentum vector evolution becomes misaligned with the singly-averaged results after several decades. For larger SRP perturbation angles, corresponding to faster precessions of the angular momentum vector, this deviation becomes more pronounced. For $\Lambda = 12.60°$, the doubly-averaged equations are able to capture the complex beating phenomenon, but predict a faster precession causing a shift in the inclination evolution.

[4]Recall that $\boldsymbol{e}\cdot\boldsymbol{h} = 0$ and $\boldsymbol{e}\cdot\boldsymbol{e} + \boldsymbol{h}\cdot\boldsymbol{h} = 1$.

[5]In our derivation of the doubly-averaged equations, we assumed the Moon followed a Keplerian ellipse about the Earth. However, in one Saros cycle the Moon completes over 200 orbits, thereby justifying our inclusion of its nodal regression into our integrations.

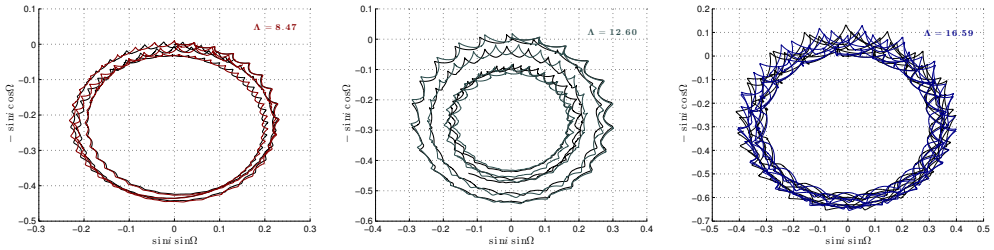

a) Angular momentum unit vector evolution. **b)** Angular momentum unit vector evolution. **c)** Angular momentum unit vector evolution.

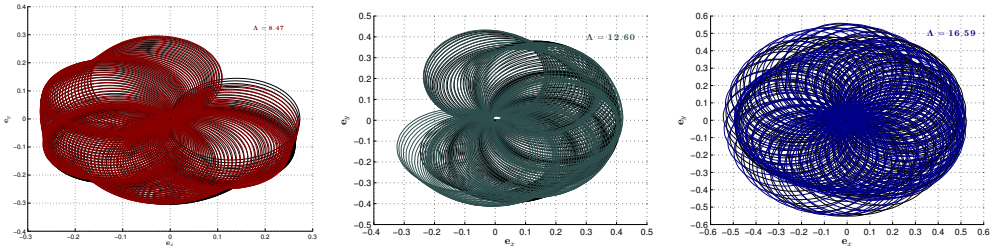

d) Eccentricity vector evolution. **e)** Eccentricity vector evolution. **f)** Eccentricity vector evolution.

Figure 3: Comparison of singly-averaged and doubly-averaged third-body dynamics for long-term propagations (100 years) over a range of Λ values. For all cases, the doubly-averaged solutions are shown in black. The singly-averaged SRP and J_2 dynamics were included in the simulations, and the position vectors of both the Sun and the Moon were computed using two-body dynamics, accounting for the lunar nodal regression.

C. Saros Resonance

Although the exact solution to the secular orbital motion is unknown, its qualitative properties are understood more easily though our formulation of the averaged equations. For certain SRP perturbation angles, the coupling between SRP, J_2 and lunisolar perturbations produce unexpectedly rich dynamical behaviors. In particular, we discovered that when the nodal rate of the system is commensurate with the nodal rate of the Moon, the perturbations build up more effectively over long periods to produce significant effects on the orbit. Such resonances, which occurs for a class of HAMR objects that are not cleared out of orbit, gives rise to strongly changing dynamics over longer time periods. This resonant behavior explains the long-term beating phenomenon that occurs for $\Lambda = 12.60°$ (see Figure 2(d)). Its nodal period in the equatorial frame is close enough to the Saros (sidereal period of nodal regression) that there is a strong interaction between the lunar effects and the overall precession rate. The orbit goes through a period where the Moon is actually systematically reducing the angular momentum or some component of it, and a period where it is farther away and increasing it.

To better understand the underlying mechanism of this resonance effect, we propagate several HAMR objects for 200 years using the initial condition given in Table 1, but varying the initial lunar node. For $\Lambda = 13.81°$, the nodal period is approximately equal to 18.61 years, thereby inducing a $1:1$ resonance with the Saros. Figure 4 shows the inclination and angular momentum vector evolution, as a function of the initial node angle. The qualitative picture of the evolution changes drastically based on this angle, which is indicative of resonance. Figures 5 and 6 shows the evolution of objects with nodal rates either too slow or too fast to resonantly interact with the Saros. The approximate range of SRP perturbation angles for which resonance can be important at GEO is between $\Lambda = 10.5°$ and $\Lambda = 15.5°$.

V. Discussion

The recognition of the Saros resonance raises many questions of interest concerning the nature and evolution of the HAMR debris population. This phenomenon actually appears in Anselmo and Pardini's[1] numerical results, and is relevant for many of the observed HAMR debris in near GEO orbits. Since the singly-averaged and, to some extent, the doubly-averaged results capture this subtle behavior, our averaged model accounts for the full dynamics precisely, and can be used for long-term predictions. The differences between the singly-averaged and doubly-averaged results is largest for HAMR objects that are caught in this resonance; as for this case, averaging over the Moon's motion may be violating the first-order averaging principle. Further analysis is needed to fully understand the resonance effect, and will be pursued in future research.

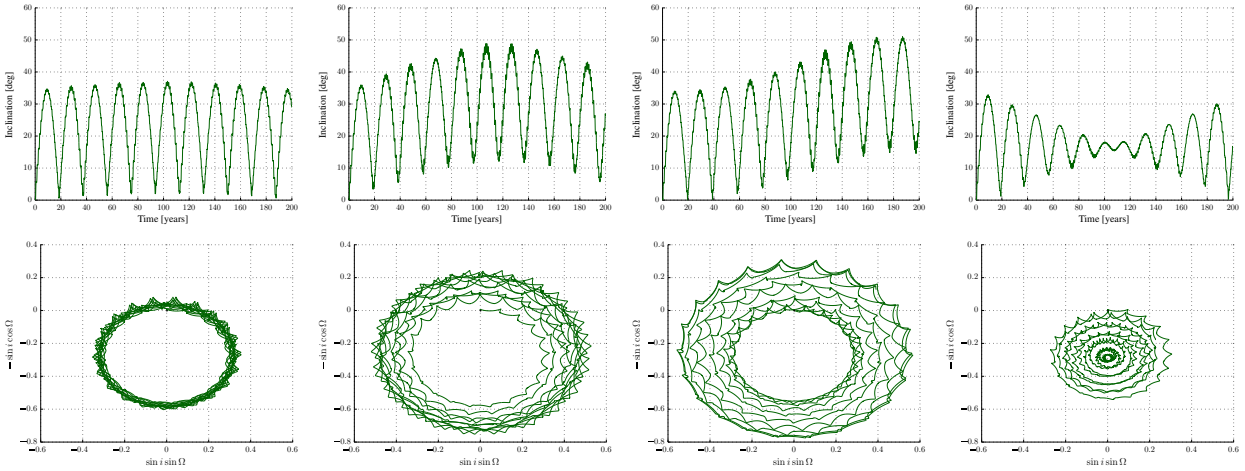

a) $\Omega_m(0) = \Omega_{m_0}$ **b)** $\Omega_m(0) = \Omega_{m_0} + \pi/2$ **c)** $\Omega_m(0) = \Omega_{m_0} + \pi$ **d)** $\Omega_m(0) = \Omega_{m_0} + 3\pi/2$

Figure 4: Long-term orbit evolution of an object with $\Lambda = 13.81°$, as a function of the initial lunar node.

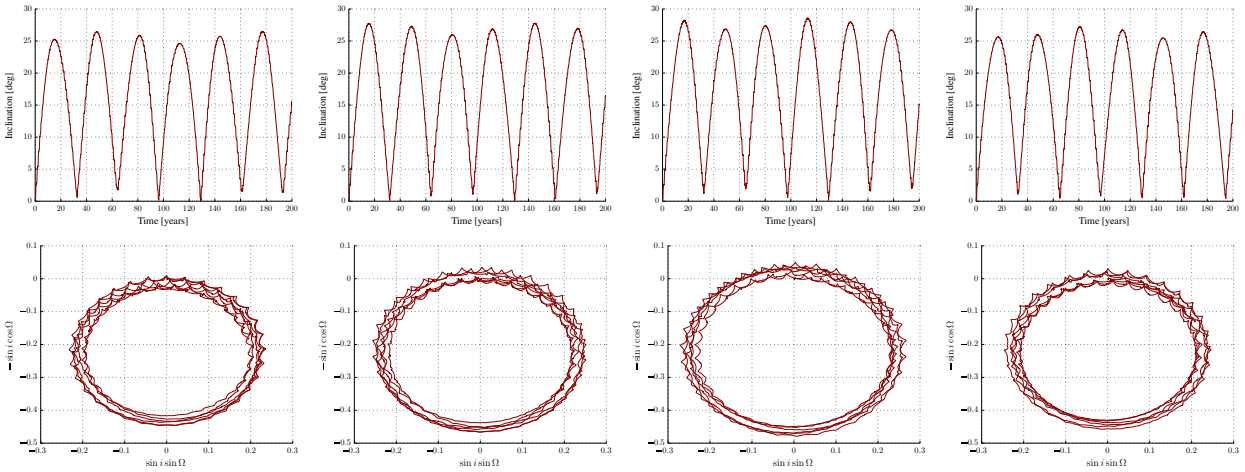

a) $\Omega_m(0) = \Omega_{m_0}$ **b)** $\Omega_m(0) = \Omega_{m_0} + \pi/2$ **c)** $\Omega_m(0) = \Omega_{m_0} + \pi$ **d)** $\Omega_m(0) = \Omega_{m_0} + 3\pi/2$

Figure 5: Long-term orbit evolution of an object with $\Lambda = 8.47°$, as a function of the initial lunar node.

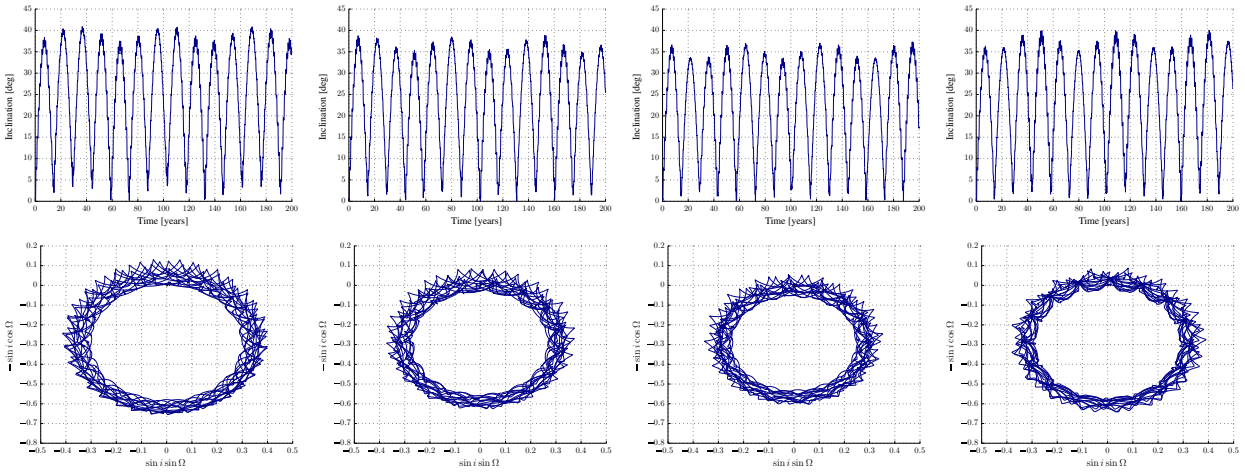

a) $\Omega_m(0) = \Omega_{m_0}$ **b)** $\Omega_m(0) = \Omega_{m_0} + \pi/2$ **c)** $\Omega_m(0) = \Omega_{m_0} + \pi$ **d)** $\Omega_m(0) = \Omega_{m_0} + 3\pi/2$

Figure 6: Long-term orbit evolution of an object with $\Lambda = 16.59°$, as a function of the initial lunar node.

The dynamic behavior underlined by our averaged theory is in good agreement with earlier researchers.[1,5,12,24] We attribute any quantitative differences between the singly-averaged and non-averaged simulations to our use of the Hill approximation for the lunar perturbing potential; namely, in the assumption that $\boldsymbol{r}/\boldsymbol{d}_m \ll 1$, which is not entirely accurate for GEO orbiting debris. However, this does not present an issue, as our theory is able to capture the extreme dynamical behaviors resulting from the complex coupling between SRP, J_2 and lunisolar perturbations.

VI. Conclusion

The contribution of our current analysis is the development of a new non-singular theory of first-order averaging explicitly given in terms of the eccentricity and angular momentum vector. This work provides a unified approach to the analysis and simulation of HAMR debris over long timespans, and allows for the qualitative nature of their evolution to be understood. We exposed the Saros resonance as an important phenomena that has not been identified previously, and which leads to complex evolutionary behaviors when the perturbing forces act in concert. This resonance may play a role in generating orbital chaos, which is a topic of future research.

We have shown that we understand every aspect of HAMR debris motion, and that by knowing the complete qualitative picture of the evolution, we can use our model to predict the population. Given that HAMR objects are the most difficult to target from an observational point of view, this work will have many implications for the space surveillance community, and will allow observers to implement better search strategies for this class of debris. The properties of the resonant population will serve as important constraints for models of its origin and evolution.

Appendices

A. Vector Kinematic Quantities

The fundamental vectors for the two-body problem, specified using the classical orbit elements relative to an inertial frame, are[20]

$$\hat{\boldsymbol{h}} = \sin i \sin\Omega \hat{\boldsymbol{x}} - \sin i \cos\Omega \hat{\boldsymbol{y}} + \cos i \hat{\boldsymbol{z}} \tag{58a}$$

$$\begin{aligned}\hat{\boldsymbol{e}} &= (\cos\omega\cos\Omega - \cos i \sin\omega \sin\Omega)\hat{\boldsymbol{x}} \\ &\quad + (\cos\omega \sin\Omega + \cos i \sin\omega\cos\Omega)\hat{\boldsymbol{y}} \\ &\quad + \sin i \sin\omega \hat{\boldsymbol{z}}\end{aligned} \tag{58b}$$

$$\hat{\boldsymbol{e}}_\perp = \tilde{\hat{\boldsymbol{h}}} \cdot \hat{\boldsymbol{e}} \tag{58c}$$

$$\begin{aligned}&= -(\sin\omega\cos\Omega + \cos i \cos\omega \sin\Omega)\hat{\boldsymbol{x}} \\ &\quad - (\sin\omega\sin\Omega - \cos i \cos\omega\cos\Omega)\hat{\boldsymbol{x}} \\ &\quad + \sin i \cos\omega \hat{\boldsymbol{z}}\end{aligned} \tag{58d}$$

B. Averaging Results

For the elliptic orbit two-body problem

$$\boldsymbol{r} = r\left[\cos f \hat{\boldsymbol{e}} + \sin f \hat{\boldsymbol{e}}_\perp\right] \tag{59}$$

$$\boldsymbol{v} = \sqrt{\frac{\mu}{a(1-e^2)}}\left[-\sin f \hat{\boldsymbol{e}} + (e + \cos f)\hat{\boldsymbol{e}}_\perp\right] \tag{60}$$

where

$$r = \frac{a(1-e^2)}{1 + e\cos f} \tag{61}$$

Although averaging is defined with respect to mean anomaly, we can compute the averages using true anomaly through the differential relationship

$$\mathrm{d}M = \frac{(1-e^2)^{3/2}}{(1+e\cos f)^2}\,\mathrm{d}f \tag{62}$$

We also have the following useful relations for the flight path angle γ:

$$\boldsymbol{r}\cdot\boldsymbol{v} = H\tan\gamma \tag{63}$$

$$\tan\gamma = \frac{e\sin f}{1 + e\cos f} \tag{64}$$

where $H = \sqrt{\mu a(1-e^2)}$ is the angular momentum of the orbit. Therefore,

$$\begin{aligned}\overline{(\boldsymbol{r}\cdot\boldsymbol{v})\boldsymbol{r}} &= \frac{1}{2\pi}\int_0^{2\pi}(\boldsymbol{r}\cdot\boldsymbol{v})\boldsymbol{r}\,\mathrm{d}M \\ &= \frac{\sqrt{\mu}a^{3/2}e(1-e^2)^3}{2\pi}\int_0^{2\pi}\left[\frac{\cos f\sin f}{(1+e\cos f)^4}\hat{\boldsymbol{e}} + \frac{\sin^2 f}{(1+e\cos f)^4}\hat{\boldsymbol{e}}_\perp\right]\mathrm{d}f\end{aligned} \tag{65}$$

Noting that the factor of $\hat{\boldsymbol{e}}$ is an odd function in true anomaly, and hence will average to zero, we obtain

$$\overline{(\boldsymbol{r}\cdot\boldsymbol{v})\boldsymbol{r}} = \frac{\sqrt{\mu}a^{3/2}e(1-e^2)^3}{2\pi}\int_0^{2\pi}\frac{\sin^2 f}{(1+e\cos f)^4}\,\mathrm{d}f\,\hat{\boldsymbol{e}}_\perp \tag{66}$$

We can expand $1/(1+e\cos f)^4$ in a Fourier series (c.f.[20]) as

$$\frac{1}{(1+e\cos f)^4} = \sum_{m=0}^{\infty} b_m^4\cos(mf) \tag{67}$$

where the coefficients have the general definitions:

$$b_0^n = \frac{\sqrt{1-e^2}}{(1-e^2)^n}f_0^n \tag{68}$$

$$b_k^n = (-1)^k 2\left(\frac{e}{2}\right)^k\frac{\sqrt{1-e^2}}{(1-e^2)^n}f_k^n \tag{69}$$

in which

$$f_k^{n+1} = \begin{cases}\dfrac{(n-k)!(n+k)!}{n!^2}\displaystyle\sum_{l=0}^{\lfloor(n-k)/2\rfloor}\frac{n!}{l!(l+k)!(n-k-2l)!}\left(\frac{e}{2}\right)^{2l} & n+1>k \\ \dfrac{n-k}{n}(1-e^2)f_k^n + 2f_{k-1}^{n+1} & n+1\leqslant k\end{cases} \tag{70}$$

$$f_k^1 = \left(\frac{2}{1+\sqrt{1-e^2}}\right)^k \tag{71}$$

where $\lfloor a\rfloor$ is the floor function and denotes the integer part of a. Substituting the expansion into Eq. 66 and applying a simple trig relation for $\sin^2 f$, we find

$$\begin{aligned}\overline{(\boldsymbol{r}\cdot\boldsymbol{v})\boldsymbol{r}} &= \frac{\sqrt{\mu}a^{3/2}e(1-e^2)^3}{4\pi}\int_0^{2\pi}[1-\cos(2f)]\sum_{m=0}^{\infty}b_m^4\cos(mf)\,\mathrm{d}f\,\hat{\boldsymbol{e}}_\perp \\ &= \frac{\sqrt{\mu}a^{3/2}e(1-e^2)^3}{2}\left(b_0^4 - \frac{1}{2}b_2^4\right)\hat{\boldsymbol{e}}_\perp\end{aligned} \tag{72}$$

where

$$b_0^4 = \frac{\sqrt{1-e^2}}{(1-e^2)^4}f_0^4, \quad b_2^4 = \frac{e^2}{2}\frac{\sqrt{1-e^2}}{(1-e^2)^4}f_2^4 \tag{73}$$

Computation of the factors yields $f_0^4 = 1+3e^2/2$ and $f_2^4 = 10$. Therefore,

$$\overline{(\boldsymbol{r}\cdot\boldsymbol{v})\boldsymbol{r}} = \frac{1}{2}\sqrt{\mu}a^{3/2}e\sqrt{1-e^2}\hat{\boldsymbol{e}}_\perp \tag{74}$$

We also require the average of the triad of position and velocity vectors $\boldsymbol{rrv}$. From Eqs. 59 and 60, this triad can be expressed in terms of the fundamental vectors

$$\begin{aligned}\boldsymbol{rrv} = rH\big[&\cos^2 f(\tan\gamma\cos f - \sin f)\hat{\boldsymbol{e}}\hat{\boldsymbol{e}}\hat{\boldsymbol{e}} + \cos f\sin f(\tan\gamma\sin f + \cos f)\hat{\boldsymbol{e}}\hat{\boldsymbol{e}}_\perp\hat{\boldsymbol{e}}_\perp \\ &+ \cos^2 f(\tan\gamma\sin f + \cos f)\hat{\boldsymbol{e}}\hat{\boldsymbol{e}}\hat{\boldsymbol{e}}_\perp + \cos f\sin f(\tan\gamma\cos f - \sin f)\hat{\boldsymbol{e}}\hat{\boldsymbol{e}}_\perp\hat{\boldsymbol{e}} \\ &+ \cos f\sin f(\tan\gamma\cos f - \sin f)\hat{\boldsymbol{e}}_\perp\hat{\boldsymbol{e}}\hat{\boldsymbol{e}} + \sin^2 f(\tan\gamma\sin f + \cos f)\hat{\boldsymbol{e}}_\perp\hat{\boldsymbol{e}}_\perp\hat{\boldsymbol{e}}_\perp \\ &+ \cos f\sin f(\tan\gamma\sin f + \cos f)\hat{\boldsymbol{e}}_\perp\hat{\boldsymbol{e}}\hat{\boldsymbol{e}}_\perp + \sin^2 f(\tan\gamma\cos f - \sin f)\hat{\boldsymbol{e}}_\perp\hat{\boldsymbol{e}}_\perp\hat{\boldsymbol{e}}\big]\end{aligned} \tag{75}$$

Noting that $\tan\gamma$ and $\sin f$ are both odd functions in true anomaly, and $\cos f$ and r are both even in true anomaly, the factors of $\hat{\boldsymbol{e}}\hat{\boldsymbol{e}}\hat{\boldsymbol{e}}$, $\hat{\boldsymbol{e}}\hat{\boldsymbol{e}}_\perp\hat{\boldsymbol{e}}_\perp$, $\hat{\boldsymbol{e}}_\perp\hat{\boldsymbol{e}}\hat{\boldsymbol{e}}_\perp$, and $\hat{\boldsymbol{e}}_\perp\hat{\boldsymbol{e}}_\perp\hat{\boldsymbol{e}}$ will be odd in true anomaly, and hence will average to zero. Therefore,

$$\begin{aligned}\overline{\boldsymbol{rrv}} &= \frac{1}{2\pi}\int_0^{2\pi} \boldsymbol{rrv}\,\mathrm{d}M \\ &= \frac{\sqrt{\mu}a^{3/2}(1-e^2)^{3/2}}{2\pi}\int_0^{2\pi}\frac{1}{1+e\cos f}\Big[\cos^2 f(\tan\gamma\sin f+\cos f)\hat{\boldsymbol{e}}\hat{\boldsymbol{e}}\hat{\boldsymbol{e}}_\perp + \cos f\sin f(\tan\gamma\cos f-\sin f)\hat{\boldsymbol{e}}\hat{\boldsymbol{e}}_\perp\hat{\boldsymbol{e}} \\ &\quad + \cos f\sin f(\tan\gamma\cos f-\sin f)\hat{\boldsymbol{e}}_\perp\hat{\boldsymbol{e}}\hat{\boldsymbol{e}} + \sin^2 f(\tan\gamma\sin f+\cos f)\hat{\boldsymbol{e}}_\perp\hat{\boldsymbol{e}}_\perp\hat{\boldsymbol{e}}_\perp\Big]\,\mathrm{d}M \end{aligned} \tag{76}$$

We compute the averages using eccentric anomaly through the relationships

$$\cos f = \frac{\cos E - e}{1-e\cos E} \tag{77}$$

$$\sin f = \frac{\sqrt{1-e^2}\sin E}{1-e\cos E} \tag{78}$$

$$\cos E = \frac{e+\cos f}{1+e\cos f} \tag{79}$$

$$\sin E = \frac{\sqrt{1-e^2}\sin f}{1+e\cos f} \tag{80}$$

$$\mathrm{d}M = (1-e\cos E)\,\mathrm{d}E \tag{81}$$

The first integral becomes

$$\begin{aligned}\int_0^{2\pi}\frac{\cos^2 f(\tan\gamma\sin f+\cos f)}{1+e\cos f}\,\mathrm{d}M &= \int_0^{2\pi}\frac{\cos^2 f}{1+e\cos f}\left(\frac{e+\cos f}{1+e\cos f}\right)\mathrm{d}M \\ &= \frac{1}{1-e^2}\int_0^{2\pi}\cos E(\cos E-e)^2\,\mathrm{d}E \\ &= -\frac{2\pi e}{1-e^2}\end{aligned} \tag{82}$$

The next integral is evaluated as

$$\begin{aligned}\int_0^{2\pi}\frac{\cos f\sin f(\tan\gamma\cos f-\sin f)}{1+e\cos f}\,\mathrm{d}M &= \int_0^{2\pi}\frac{\cos f\sin f}{1+e\cos f}\left(-\frac{\sin f}{1+e\cos f}\right)\mathrm{d}M \\ &= -\int_0^{2\pi}\left[\cos E-\frac{e(1-e\cos E)}{1-e^2}\right]\sin^2 E\,\mathrm{d}E \\ &= \frac{e}{1-e^2}\int_0^{2\pi}(1-e\cos E)\sin^2 E\,\mathrm{d}E \\ &= \frac{\pi e}{1-e^2}\end{aligned} \tag{83}$$

And the final integral is

$$\begin{aligned}\int_0^{2\pi}\frac{\sin^2 f(\tan\gamma\sin f+\cos f)}{1+e\cos f}\,\mathrm{d}M &= \int_0^{2\pi}\frac{\sin^2 f}{1+e\cos f}\left(\frac{e+\cos f}{1+e\cos f}\right)\mathrm{d}M \\ &= \int_0^{2\pi}\cos E\sin^2 E\,\mathrm{d}E \\ &= 0\end{aligned} \tag{84}$$

Substituting these results into Eq. 76 gives

$$\overline{\boldsymbol{rrv}} = \frac{1}{2}\sqrt{\mu}a^{3/2}e\sqrt{1-e^2}(-2\hat{\boldsymbol{e}}\hat{\boldsymbol{e}}\hat{\boldsymbol{e}}_\perp + \hat{\boldsymbol{e}}\hat{\boldsymbol{e}}_\perp\hat{\boldsymbol{e}} + \hat{\boldsymbol{e}}_\perp\hat{\boldsymbol{e}}\hat{\boldsymbol{e}}) \tag{85}$$

C. Third-body Doubly-averaged Orbital Element Rates

The perturbation equations for the classical orbital elements can be expressed in terms of the vectors $\boldsymbol{h}$ and $\boldsymbol{e}$ using vector calculus. Namely,

$$\dot{e} = \hat{\boldsymbol{e}} \cdot \dot{\boldsymbol{e}} \tag{86}$$

where (=) on $\dot{\boldsymbol{e}}$ has been dropped for convenience. Substituting Eq. 55 for $\dot{\boldsymbol{e}}$ gives

$$\begin{aligned}\dot{e} &= -\frac{3\mu_p}{4na_p^3(1-e_p^2)^{3/2}}\left\{4(\boldsymbol{e}\cdot\hat{\boldsymbol{H}}_p)\hat{\boldsymbol{e}}\cdot\tilde{\boldsymbol{h}}\cdot\hat{\boldsymbol{H}}_p - \hat{\boldsymbol{e}}\cdot\tilde{\boldsymbol{h}}\cdot\boldsymbol{e} - (\tilde{\boldsymbol{h}}\cdot\boldsymbol{e}\cdot\hat{\boldsymbol{H}}_p)\hat{\boldsymbol{e}}\cdot\hat{\boldsymbol{H}}_p\right\} \\ &= \frac{15e\sqrt{1-e^2}\mu_p}{4na_p^3(1-e_p^2)^{3/2}}(\hat{\boldsymbol{e}}\cdot\hat{\boldsymbol{H}}_p)(\hat{\boldsymbol{e}}_\perp\cdot\hat{\boldsymbol{H}}_p)\end{aligned} \tag{87}$$

Recalling that $\cos i = \hat{\boldsymbol{h}}\cdot\hat{\boldsymbol{H}}_p$, the secular rate for inclination is found by differentiating both sides of the relation

$$-\sin i\,\dot{i} = \dot{\hat{\boldsymbol{h}}}\cdot\hat{\boldsymbol{H}}_p \tag{88}$$

where $\dot{\hat{\boldsymbol{h}}}$ is found through $\boldsymbol{h}$ and $\dot{\boldsymbol{h}}$

$$\dot{\hat{\boldsymbol{h}}} = \frac{e\dot{e}}{1-e^2}\hat{\boldsymbol{h}} + \frac{1}{\sqrt{1-e^2}}\dot{\boldsymbol{h}} \tag{89}$$

Therefore,

$$-\sin i\,\dot{i} = \frac{e\dot{e}}{1-e^2}(\hat{\boldsymbol{h}}\cdot\hat{\boldsymbol{H}}_p) + \frac{1}{\sqrt{1-e^2}}(\dot{\boldsymbol{h}}\cdot\hat{\boldsymbol{H}}_p) \tag{90}$$

Noting that $\dot{\boldsymbol{h}}\cdot\hat{\boldsymbol{H}}_p = 0$ and substituting Eq. 87 for $\dot{e}$ yields

$$-\sin i\,\dot{i} = \frac{15e^2\mu_p}{4n\sqrt{1-e^2}a_p^3(1-e_p^2)^{3/2}}(\hat{\boldsymbol{h}}\cdot\hat{\boldsymbol{H}}_p)(\hat{\boldsymbol{e}}\cdot\hat{\boldsymbol{H}}_p)(\hat{\boldsymbol{e}}_\perp\cdot\hat{\boldsymbol{H}}_p) \tag{91}$$

Consequently,

$$\dot{i} = -\frac{15e^2\mu_p}{4n\sqrt{1-e^2}a_p^3(1-e_p^2)^{3/2}}(\hat{\boldsymbol{h}}\cdot\hat{\boldsymbol{H}}_p)(\hat{\boldsymbol{e}}\cdot\hat{\boldsymbol{H}}_p)(\hat{\boldsymbol{e}}\cdot\hat{\boldsymbol{n}}) \tag{92}$$

The longitude of the ascending node is given by

$$\tan\Omega = \frac{\hat{\boldsymbol{h}}\cdot\hat{\boldsymbol{E}}_p}{-\hat{\boldsymbol{h}}\cdot\hat{\boldsymbol{E}}_{p_\perp}} \tag{93}$$

Differentiating with respect to time, we find

$$\frac{1}{\cos^2\Omega}\dot{\Omega} = \frac{-(\hat{\boldsymbol{h}}\cdot\hat{\boldsymbol{E}}_{p_\perp})(\dot{\hat{\boldsymbol{h}}}\cdot\hat{\boldsymbol{E}}_p) + (\hat{\boldsymbol{h}}\cdot\hat{\boldsymbol{E}}_p)(\dot{\hat{\boldsymbol{h}}}\cdot\hat{\boldsymbol{E}}_{p_\perp})}{(\hat{\boldsymbol{h}}\cdot\hat{\boldsymbol{E}}_{p_\perp})^2} \tag{94}$$

in which we note

$$\begin{aligned}\dot{\hat{\boldsymbol{h}}}\cdot\hat{\boldsymbol{E}}_p &= \frac{e\dot{e}}{1-e^2}\hat{\boldsymbol{h}}\cdot\hat{\boldsymbol{E}}_p + \frac{1}{\sqrt{1-e^2}}\dot{\boldsymbol{h}}\cdot\hat{\boldsymbol{E}}_p \\ &= \frac{3\mu_p}{4n\sqrt{1-e^2}a_p^3(1-e_p^2)^{3/2}}\left[5e^2(\hat{\boldsymbol{h}}\cdot\hat{\boldsymbol{E}}_p)(\hat{\boldsymbol{e}}\cdot\hat{\boldsymbol{H}}_p)(\hat{\boldsymbol{e}}_\perp\cdot\hat{\boldsymbol{H}}_p) - \hat{\boldsymbol{H}}_p\cdot[5\boldsymbol{e}\boldsymbol{e} - \boldsymbol{h}\boldsymbol{h}]\cdot\hat{\boldsymbol{E}}_{p_\perp}\right]\end{aligned} \tag{95}$$

$$\begin{aligned}\dot{\hat{\boldsymbol{h}}}\cdot\hat{\boldsymbol{E}}_{p_\perp} &= \frac{e\dot{e}}{1-e^2}\hat{\boldsymbol{h}}\cdot\hat{\boldsymbol{E}}_{p_\perp} + \frac{1}{\sqrt{1-e^2}}\dot{\boldsymbol{h}}\cdot\hat{\boldsymbol{E}}_{p_\perp} \\ &= \frac{3\mu_p}{4n\sqrt{1-e^2}a_p^3(1-e_p^2)^{3/2}}\left[5e^2(\hat{\boldsymbol{h}}\cdot\hat{\boldsymbol{E}}_{p_\perp})(\hat{\boldsymbol{e}}\cdot\hat{\boldsymbol{H}}_p)(\hat{\boldsymbol{e}}_\perp\cdot\hat{\boldsymbol{H}}_p) + \hat{\boldsymbol{H}}_p\cdot[5\boldsymbol{e}\boldsymbol{e} - \boldsymbol{h}\boldsymbol{h}]\cdot\hat{\boldsymbol{E}}_p\right]\end{aligned} \tag{96}$$

Therefore, the numerator on the right-hand side of Eq. 94 becomes

$$
\begin{aligned}
-(\hat{\boldsymbol{h}}\cdot\hat{\boldsymbol{E}}_{p_\perp})(\dot{\hat{\boldsymbol{h}}}\cdot\hat{\boldsymbol{E}}_p)+(\hat{\boldsymbol{h}}\cdot\hat{\boldsymbol{E}}_p)(\dot{\hat{\boldsymbol{h}}}\cdot\hat{\boldsymbol{E}}_{p_\perp}) &= \frac{3\mu_p}{4n\sqrt{1-e^2}a_p^3(1-e_p^2)^{3/2}}\Big\{(\hat{\boldsymbol{h}}\cdot\hat{\boldsymbol{E}}_{p_\perp})\hat{\boldsymbol{H}}_p\cdot[5\boldsymbol{ee}-\boldsymbol{hh}]\cdot\hat{\boldsymbol{E}}_{p_\perp} \\
&\quad +(\hat{\boldsymbol{h}}\cdot\hat{\boldsymbol{E}}_p)\hat{\boldsymbol{H}}_p\cdot[5\boldsymbol{ee}-\boldsymbol{hh}]\cdot\hat{\boldsymbol{E}}_p\Big\} \\
&= -\frac{3\mu_p}{4n\sqrt{1-e^2}a_p^3(1-e_p^2)^{3/2}}(\hat{\boldsymbol{h}}\cdot\hat{\boldsymbol{H}}_p) \\
&\quad \Big[5(\boldsymbol{e}\cdot\hat{\boldsymbol{H}}_p)^2+(\boldsymbol{h}\cdot\hat{\boldsymbol{E}}_p)^2+(\boldsymbol{h}\cdot\hat{\boldsymbol{E}}_{p_\perp})^2\Big] \qquad (97)
\end{aligned}
$$

Consequently,

$$
\begin{aligned}
\dot{\Omega} &= -\frac{3\mu_p}{4n\sqrt{1-e^2}a_p^3(1-e_p^2)^{3/2}}(\hat{\boldsymbol{h}}\cdot\hat{\boldsymbol{H}}_p)\Big[5(\boldsymbol{e}\cdot\hat{\boldsymbol{H}}_p)^2+(\boldsymbol{h}\cdot\hat{\boldsymbol{E}}_p)^2+(\boldsymbol{h}\cdot\hat{\boldsymbol{E}}_{p_\perp})^2\Big]\frac{\cos^2\Omega}{(\hat{\boldsymbol{h}}\cdot\hat{\boldsymbol{E}}_{p_\perp})^2} \\
&= -\frac{3\mu_p}{4n\sqrt{1-e^2}a_p^3(1-e_p^2)^{3/2}}(\hat{\boldsymbol{h}}\cdot\hat{\boldsymbol{H}}_p)\Big[5(\boldsymbol{e}\cdot\hat{\boldsymbol{H}}_p)^2+(\boldsymbol{h}\cdot\hat{\boldsymbol{E}}_p)^2+(\boldsymbol{h}\cdot\hat{\boldsymbol{E}}_{p_\perp})^2\Big]\frac{1}{\sin^2 i} \\
&= -\frac{3\mu_p}{4n\sqrt{1-e^2}a_p^3(1-e_p^2)^{3/2}}(\hat{\boldsymbol{h}}\cdot\hat{\boldsymbol{H}}_p)\left[1+4e^2-5e^2(\hat{\boldsymbol{e}}\cdot\hat{\boldsymbol{n}})^2\right] \qquad (98)
\end{aligned}
$$

The secular equation for the argument of periapsis is obtained by differentiating $\cos\omega=\hat{\boldsymbol{e}}\cdot\hat{\boldsymbol{n}}$ as

$$
-\sin\omega\,\dot{\omega}=\hat{\boldsymbol{e}}\cdot\dot{\hat{\boldsymbol{n}}}+\dot{\hat{\boldsymbol{e}}}\cdot\hat{\boldsymbol{n}} \qquad (99)
$$

where, from Eqs. 55 and 87, we have

$$
\begin{aligned}
\dot{\hat{\boldsymbol{e}}} &= \frac{\dot{\boldsymbol{e}}-\dot{e}\hat{\boldsymbol{e}}}{e} \qquad (100) \\
&= \frac{3\sqrt{1-e^2}\mu_p}{4na_p^3(1-e_p^2)^{3/2}}\Big\{(\hat{\boldsymbol{e}}\cdot\hat{\boldsymbol{H}}_p)\tilde{\hat{\boldsymbol{h}}}\cdot\hat{\boldsymbol{H}}_p+\tilde{\hat{\boldsymbol{h}}}\cdot\hat{\boldsymbol{e}}+(\tilde{\hat{\boldsymbol{h}}}\cdot\hat{\boldsymbol{e}}\cdot\hat{\boldsymbol{H}}_p)\hat{\boldsymbol{H}}_p+5(\hat{\boldsymbol{e}}\cdot\hat{\boldsymbol{H}}_p)^2\hat{\boldsymbol{e}}_\perp\Big\} \qquad (101)
\end{aligned}
$$

Moreover,

$$
\dot{\hat{\boldsymbol{e}}}\cdot\hat{\boldsymbol{n}}=\frac{3\sqrt{1-e^2}\mu_p}{4na_p^3(1-e_p^2)^{3/2}}\left[(\hat{\boldsymbol{e}}\cdot\hat{\boldsymbol{H}}_p)\tilde{\hat{\boldsymbol{h}}}\cdot\hat{\boldsymbol{n}}\cdot\hat{\boldsymbol{H}}_p+\tilde{\hat{\boldsymbol{h}}}\cdot\hat{\boldsymbol{e}}\cdot\hat{\boldsymbol{n}}+5(\hat{\boldsymbol{e}}\cdot\hat{\boldsymbol{H}}_p)^2\hat{\boldsymbol{e}}_\perp\cdot\hat{\boldsymbol{n}}\right] \qquad (102)
$$

Since the node vector is only a function of Ω, we have

$$
\dot{\hat{\boldsymbol{n}}}=\dot{\Omega}(-\sin\Omega\hat{\boldsymbol{E}}_p+\cos\Omega\hat{\boldsymbol{E}}_{p_\perp}) \qquad (103)
$$

Therefore,

$$
\begin{aligned}
\hat{\boldsymbol{e}}\cdot\dot{\hat{\boldsymbol{n}}} &= \cos i\sin\omega\,\dot{\Omega} \qquad (104) \\
&= -\frac{3\mu_p}{4n\sqrt{1-e^2}a_p^3(1-e_p^2)^{3/2}}\sin\omega(\hat{\boldsymbol{h}}\cdot\hat{\boldsymbol{H}}_p)^2\left[1+4e^2-5e^2(\hat{\boldsymbol{e}}\cdot\hat{\boldsymbol{n}})^2\right] \qquad (105)
\end{aligned}
$$

Hence, the secular effect of the perturbation on the augment of periapsis is

$$
\begin{aligned}
\dot{\omega} &= \frac{3\mu_p}{4n\sqrt{1-e^2}a_p^3(1-e_p^2)^{3/2}}\Big\{(\hat{\boldsymbol{h}}\cdot\hat{\boldsymbol{H}}_p)^2\left[1+4e^2-5e^2(\hat{\boldsymbol{e}}\cdot\hat{\boldsymbol{n}})^2\right] \\
&\quad -\frac{1-e^2}{\sin\omega}\left[(\hat{\boldsymbol{e}}\cdot\hat{\boldsymbol{H}}_p)\tilde{\hat{\boldsymbol{h}}}\cdot\hat{\boldsymbol{n}}\cdot\hat{\boldsymbol{H}}_p+\tilde{\hat{\boldsymbol{h}}}\cdot\hat{\boldsymbol{e}}\cdot\hat{\boldsymbol{n}}+5(\hat{\boldsymbol{e}}\cdot\hat{\boldsymbol{H}}_p)^2\hat{\boldsymbol{e}}_\perp\cdot\hat{\boldsymbol{n}}\right]\Big\} \\
&= \frac{3\mu_p}{4n\sqrt{1-e^2}a_p^3(1-e_p^2)^{3/2}}\left[2+3e^2-5(\hat{\boldsymbol{e}}\cdot\hat{\boldsymbol{H}}_p)^2-5e^2(\hat{\boldsymbol{e}}\cdot\hat{\boldsymbol{n}})^2\right] \qquad (106)
\end{aligned}
$$

Acknowledgements

This material is based upon work supported by the National Science Foundation Graduate Research Fellowship under Grant No. DGE 1144083. Any opinions, findings, and conclusions or recommendations expressed in this material are those of the authors and do not necessarily reflect the views of the National Science Foundation.

Daniel J. Scheeres acknowledges support from grant FA9550-11-1-0188, administered by the Air Force Office of Scientific Research.

References

[1]Anselmo, L., and Pardini, C., "Long-term dynamical evolution of high area-to-mass ratio debris released into high earth Orbits," *Acta Astronautica*, 67: 204-216, 2010.

[2]Bogoliubov, N. N., and Mitropolsky, Y. A., *Asymptotic Methods in the Theory of Non-Linear Oscillations*, Gordon and Breach, 1961.

[3]Cefola, P. J., Long, A. C., and Holloway, G., "The Long-Term Prediction of Artificial Satellite Orbits," Presented at the *AIAA 12th Aerospace Sciences Meeting*, Washington, D.C., Paper 74-170, 1974.

[4]Cefola, P.J., Sabol, C., Hill, K., and Nishimoto, D., "Demonstration of the DSST State Transition Matrix Time-Update Properties Using the Linux GTDS Program," Presented at the *Advanced Maui Optical and Space Surveillance Technologies Conference*, Maui, Hawaii, 2011.

[5]Chao, C. C., "Analytical Investigation of GEO Debris with High Area-to-Mass Ratio," Presented at the *AIAA/AAS Astrodynamics Specialist Conference*, Keystone, Colorado, Paper AIAA-2006-6514, 2006.

[6]Folkner, W. M., Williams, J. G., and Boggs, D. H., "The Planetary and Lunar Ephemeris DE 421," *The Interplanetary Network Progress Report*, 42-178, 2009.

[7]Fonte, D.J., *Implementing a 50×50 Gravity Field Model in an Orbit Determination System*, M.S. Thesis, Department of Aeronautics and Astronautics, MIT, 1993.

[8]Hu, W., and Scheeres, D. J., "Spacecraft Motion About Slowly Rotating Asteroids," *Journal of Guidance, Control, and Dynamics*, 25(4): 765-775, 2002.

[9]Kyrloff, N., and Bogoliuboff, N., *Introduction to Non-Linear Mechanics*, Princeton University Press, 1947.

[10]Lemaître, A., Delsate, N., and Valk, S., "A web of secondary resonances for large A/m geostationary debris," *Celestial Mechanics and Dynamical Astronomy*, 104: 383-402, 2009.

[11]Lidov, M. L., "Evolution of Orbits of Planetary Artificial Satellites Under the Influence of Gravitational Disturbances of Outer Bodies," *Iskusstvennye Sputniki Zemli*, 8: 1-45, 1961 [Russian]. *Artificial Earth Satellites*, 8: 168-207, 1962.

[12]Liou, J. -C., and Weaver, J. K., "Orbital Dynamics of High Area-to-Mass Ratio Debris and Their Distribution in the Geosynchronous Region," Proceedings of the *Fourth European Conference on Space Debris*, Darmstadt, Germany, Paper ESA SP-587, 2005.

[13]Lorell, J., and Anderson, J., "Precession rates for an artificial satellite," Presented at the 13th *International Astronautical Congress*, Varna, Bulgaria, 1962.

[14]McClain, W. D., "A Recursively Formulated First-Order Semianalytic Artificial Satellite Theory Based on the Generalized Method of Averaging," *Computer Sciences Corporation*, Report CSC/TR-77/6010 [in 1992, Wayne McClain updated the blue book. This revised version has been scanned and is available as an electronic document], Volume 1, 1977.

[15]Mignard, F. and Hénon, M. "About an Unsuspected Integrable Problem," *Celestial Mechanics and Dynamical Astronomy* 33: 239-250, 1984.

[16]Perozzi, E., Roy, A. E., Steves, B. A., and Valsecchi, G. B., "Significant High Number of Commensurabilities in the Main Lunar Problem. I: The Saros as a Near-Periodicity of the Moon's Orbit," *Celestial Mechanics and Dynamical Astronomy*, 52: 241-261, 1991.

[17]Richter, K., and Keller, H. U., "On the Stability of Dust Particle Orbits around Cometary Nuclei," *Icarus*, 114: 355-371, 1995.

[18]Rosengren, A., and Scheeres, D., "Averaged Dynamics of HAMR Objects: Effects of Attitude and Earth Oblateness," Presented at the *AAS/AIAA Astrodynamics Specialist Conference*, Girdwood, Alaska, Paper AAS 11-594, 2011.

[19]Scheeres, D. J., "Orbit Mechanics About Small Solar System Bodies," *Journal of Guidance, Control and Dynamics*, In Press. Originally presented at the *AAS/AIAA Space Flight Mechanics Meeting*, Savannah, Georgie, Paper AAS 09-220, 2009.

[20]Scheeres, D. J., *Orbital Motion in Strongly Perturbed Environments: Applications to Asteroid, Comet and Planetary Satellite Orbiters*, Springer Praxis, 2012

[21]Scheeres, D., Rosengren, A., and McMahon, J., "The Dynamics of High Area-to-Mass Ratio Objects in Earth Orbit: The Effect of Solar Radiation Pressure," Presented at the *AAS/AIAA Space Flight Mechanics Meeting*, New Orleans, Louisiana, Paper AAS 11-178, 2011.

[22]Schildknecht, T., Musci, R., Ploner, M., Beutler, G., Flury, W., Kuusela, J., de Leon Cruz, J., and de Fatima Domingueq Palmero, L., "Optical observations of space debris in GEO and in highly-eccentric orbits," *Advances in Space Research*, 34: 901-911, 2004.

[23]Struble, R. A., "An Appplication of the Method of Averaging in the Theory of Satellite Motion," *Journal of Mathematics and Mechanics*, 10: 691-704, 1961.

[24]Valk, S., Lemaître, A., and Anselmo, L., "Analytical and semi-analytical investigations of geosynchronous space debris with high area-to-mass ratios," *Advances in Space Research*, 41: 1077-1090, 2008.